Hassan Yousefi Halvaei

Optical Sensing Technologies: A Literature Review, Multi-Dimensional Taxonomy, and Case Study on Seabed Sediment Temperature Monitoring

Application to the Suvilahti Sediment Heat System, Vaasa, Finland

School of Technology and innovation
Master's thesis
Industrial Systems Analytics

Vaasa 2026

Preface

Financial support for the current master's thesis was provided by The Foundation for the Theory of Knowledge and Information, and I am sincerely grateful for the funding that made this research possible. I would also like to extend my heartfelt thanks to my supervisor, Petri Välisuo, for being a reliable guide throughout the entire research process. In addition, I am grateful to Timo Mantere and Emmanuel Nzibah for their valuable feedback and useful suggestions during this work.

Vaasa, May 2026

Hassan Yousefi Halvaei

UNIVERSITY OF VAASA
School of Technology and Innovation
Author: Hassan Yousefi Halvaei
Title of the thesis: Optical Sensing Technologies: A Literature Review, Multi-Dimensional Taxonomy, and Case Study on Seabed Sediment Temperature Monitoring
Degree: Master of Science in Technology
Degree Programme: Industrial Systems Analytics
Supervisor: Petri Välisuo, Timo Mantere
Year: 2026 **Pages:** 75

ABSTRACT:

With the rapid growth of digitalization, there is an increasing demand for accurate, high-resolution, and real-time sensing technologies capable of measuring a wide range of parameters in industrial, environmental, and energy systems. Among the available solutions, optical sensing technologies have become particularly attractive due to their high sensitivity, wide measurement range, capability for remote and distributed sensing, and immunity to electromagnetic interference. However, the broad diversity of sensing mechanisms, hardware architectures, and application areas has made it difficult to systematically compare technologies and select the most suitable solution for a given application. Currently, there is still no classification method that provides a comprehensive multi-dimensional framework for organizing optical sensing technologies.

This thesis addresses that gap by making two major contributions. First, a systematic literature review of current classification methods has been conducted and subsequently, a multi-dimensional taxonomy of optical sensing technologies has been developed. The suggested taxonomy consists of four major categories. The first one concerns the way that optical signal encodes information. The second category deals with physical interaction of light with matter. The third category categorizes the sensors depending on their physical realization and implementation platform. Finally, the fourth category considers these technologies from their applications point of view. Second, a case study has been conducted to assess the applicability of Raman-backscatter DTS in practice. The study is based on field measurement data collected at the Suvilahti seabed sediment heat system located at the west coast of Vaasa, Finland. This is the first geothermal plant in Finland that uses the seabed sediment heat as a major source of energy for urban heating purposes. Temperature profiles along two heat-collection lines have been analyzed through different seasons and years. The analysis discovers four distinct thermal zones along the sediment field, each exhibiting different seasonal temperature variation and heat extraction behaviour. The findings show that DTS technology can accurately identify small spatial and temporal temperature gradients within a marine environment and provide information that can be used in the practical management of geothermal systems based on sediments.

The outcomes of the thesis provide a structured descriptive language for optical sensing domain as well as a proven approach to measurement in urban geothermal sensing, with identified directions for future research including the application of fiber-optic current sensors to DC current measurement in data center power distribution infrastructure.

KEYWORDS: Optical Sensing, Fiber Optic Sensors, Distributed Temperature Sensing, Taxonomy, Seabed Sediment, Geothermal Energy, Raman Backscattering

Abbreviation	Full Form
AC	Alternating Current
AOF-XBT	All-Fiber Expendable Bathythermograph
APD	Avalanche Photodiode
BFS	Brillouin Frequency Shift
BOTDA	Brillouin Optical Time Domain Analysis
BOTDR	Brillouin Optical Time Domain Reflectometry
CCD	Charge-Coupled Device
CMOS	Complementary Metal-Oxide Semiconductor
CRDS	Cavity Ring-Down Spectroscopy
DAQ	Data Acquisition
DAS	Distributed Acoustic Sensing
DC	Direct Current
DFG	Difference Frequency Generation
DIAL	Differential Absorption LiDAR
DOAS	Differential Optical Absorption Spectroscopy
DOFS	Distributed Fiber-Optic Sensing System
DSP	Digital Signal Processor
DSS	Distributed Strain Sensing
DSTS	Distributed Strain and Temperature Sensing
DTS	Distributed Temperature Sensing
EFOS	Extrinsic Fiber Optic Sensor
EMI	Electromagnetic Interference
FBG	Fiber Bragg Grating
FLRD	Fiber Loop Ring-Down
FOCS	Fiber Optic Current Sensor
FPI	Fabry-Pérot Interferometer
FTIR	Fourier Transform Infrared Spectroscopy
GIC	Geomagnetically Induced Current
HDD	Horizontal Directional Drilling
HSI	Hyperspectral Imaging
HVDC	High-Voltage Direct Current
IFOS	Intrinsic Fiber Optic Sensor
IR	Infrared

ITER	International Thermonuclear Experimental Reactor
LF-DAS	Low-Frequency Distributed Acoustic Sensing
LIBS	Laser-Induced Breakdown Spectroscopy
LIDAR	Light Detection and Ranging
LIGO	Laser Interferometer Gravitational-Wave Observatory
LPG	Long Period Grating
LPFG	Long-Period Fiber Grating
LSPR	Localized Surface Plasmon Resonance
MCG	Magnetocardiography
MEG	Magnetoencephalography
MIR	Mid-Infrared Spectroscopy
MRI	Magnetic Resonance Imaging
MZI	Mach-Zehnder Interferometer
NDIR	Non-Dispersive Infrared
NIR	Near-Infrared
NIRS	Near-Infrared Spectroscopy System
NV	Nitrogen-Vacancy (centre in diamond)
OCT	Optical Coherence Tomography
ODMR	Optically Detected Magnetic Resonance
OFDR	Optical Frequency Domain Reflectometry
OTDR	Optical Time Domain Reflectometry
P-OFDR	Distributed Polarimetric Optical Frequency Domain Reflectometry
PAM	Passive Acoustic Monitoring
PALM	Photoactivated Localization Microscopy
PCA	Principal Component Analysis
PCF	Photonic Crystal Fiber
PL	Photoluminescence
PLS	Partial Least Squares
PMF	Polarization-Maintaining Fiber
POF	Plastic Optical Fiber
PRISMA	Preferred Reporting Items for Systematic Reviews and Meta-Analyses
REFLA	Branded flower cross-section heat collector pipe system (Suvilahti)
RIU	Refractive Index Unit
SFG	Sum Frequency Generation

SIM	Structured Illumination Microscopy
SMF	Single-Mode Fiber
SNR	Signal-to-Noise Ratio
SOP	State of Polarization
SPR	Surface Plasmon Resonance
STED	Stimulated Emission Depletion Microscopy
STORM	Stochastic Optical Reconstruction Microscopy
TDLAS	Tunable Diode Laser Absorption Spectroscopy
UV	Ultraviolet
UV-VIS	Ultraviolet-Visible Spectroscopy
VIS	Visible (spectrum)
VIS-NIR	Visible and Near-Infrared Spectroscopy
VOC	Volatile Organic Compound
VSFG	Vibrational Sum Frequency Generation
WDM	Wavelength Division Multiplexor

Contents

Figures

Tables

1 Introduction

With the rising use of digitalization in the industrial process and environment-related systems, there has been an increased demand for data that is accurate, real-time, and high resolution(da Costa et al., 2024, p. 1). In this context, the importance of sensing technology cannot be overstated as it is the primary source where the physical phenomena can be turned into tangible data. As far as the various types of sensing technologies available today are concerned, the application of optical sensors has proven invaluable owing to the high-resolution and quick data acquisition capabilities of these sensors (Meng et al., 2026a, p. 158). Optical sensors are inherently robust with a fast response speed that is not affected by any form of drift (Pathak & Viphavakit, 2022, p. 2).

Optical sensing involves techniques which use light-matter interactions to measure physical, chemical, and environmental parameters accurately. The technique is currently being used in various applications including process control in industries, environmental analysis, agriculture, and power systems (Wadi Harun, 2025, p. 39). In this regard, distributed fiber-optic sensors allow distributed and real-time measurement of data at several locations. These kinds of sensors have been found advantageous especially due to their ability to provide scalable, sensitive, and continuous data measurement (Udd & Jr, 2024, p. 2). Optical sensor data, usually collected through spectral readings, are generally multi-dimensional and informative (Bian et al., 2024, p. 73). In conjunction with data analysis and machine learning processes, the data can be translated into useful insights for monitoring and decision-making (Mia et al., 2026, p. 2).

However, the diverse nature of these optical sensing devices makes it difficult for researchers to understand their capabilities, limitations, and applicability across different contexts. Therefore, there is a need for a structured approach to classify and evaluate these technologies, as well as to demonstrate their practical value through data-driven analysis.

1.1 Background of Study

The optical sensors are the group of sensors that have gained popularity when applied in analysis tasks like environmental monitoring and health care purposes. This is mainly because of the easy concept behind it and the simplicity in its construction (Sing Muk, 2019, p. 270). The typical structure of an optical sensor comprises of a light source, a sensor component, light waveguide, light detector and the data processor(Sabri et al., 2013, p. 1). The main concept behind the functioning of this type of sensor relies on the detection of the variation in the behavior of light when the sensors are exposed to the analyte. The variation could be due to the alteration in the intensity or wavelength of light.

1.2 Fiber-Optical Sensing: Fundamentals and Distributed Types

Fiber optics is one of the major technologies that has made remarkable advancements in the last 25 years (Sabri et al., 2013, p. 1). Optical fiber sensors make use of the interactions between light and the material properties of the fiber to perform accurate measurements (Khonina et al., 2023, p. 2). There are several factors that have contributed to the extensive use of optical fibers in the past few decades due to their many benefits such as compactness, robustness against electromagnetic interference, adaptability, simple manufacturing, remote sensing, and anti-corrosion properties. Optical fibers find applications in the geotechnical industry, maritime industry, and power generation industry (Mahmud et al., 2024, p. 23376).

The underlying principle of operation of optical fiber sensors lies in the changes that physical properties such as temperature, stress, pressure, and vibration induce on the optical properties of a propagating light wave. The strength of the optical fiber sensor lies in its ability to use this principle in an extension along the whole length of the fiber. This makes an optical fiber the ideal medium to employ the distributed sensing concept (Katrenova et al., 2024, p. 1). From a practical standpoint, the replacement of thousands

of individual sensors with one fiber becomes possible. Optical fiber sensors enable fully distributed sensing with measurement points as close as less than 1 mm, while the fiber's thinness and flexibility ensure a wide variety of possible installation configurations (Bado & Casas, 2021, p. 2).

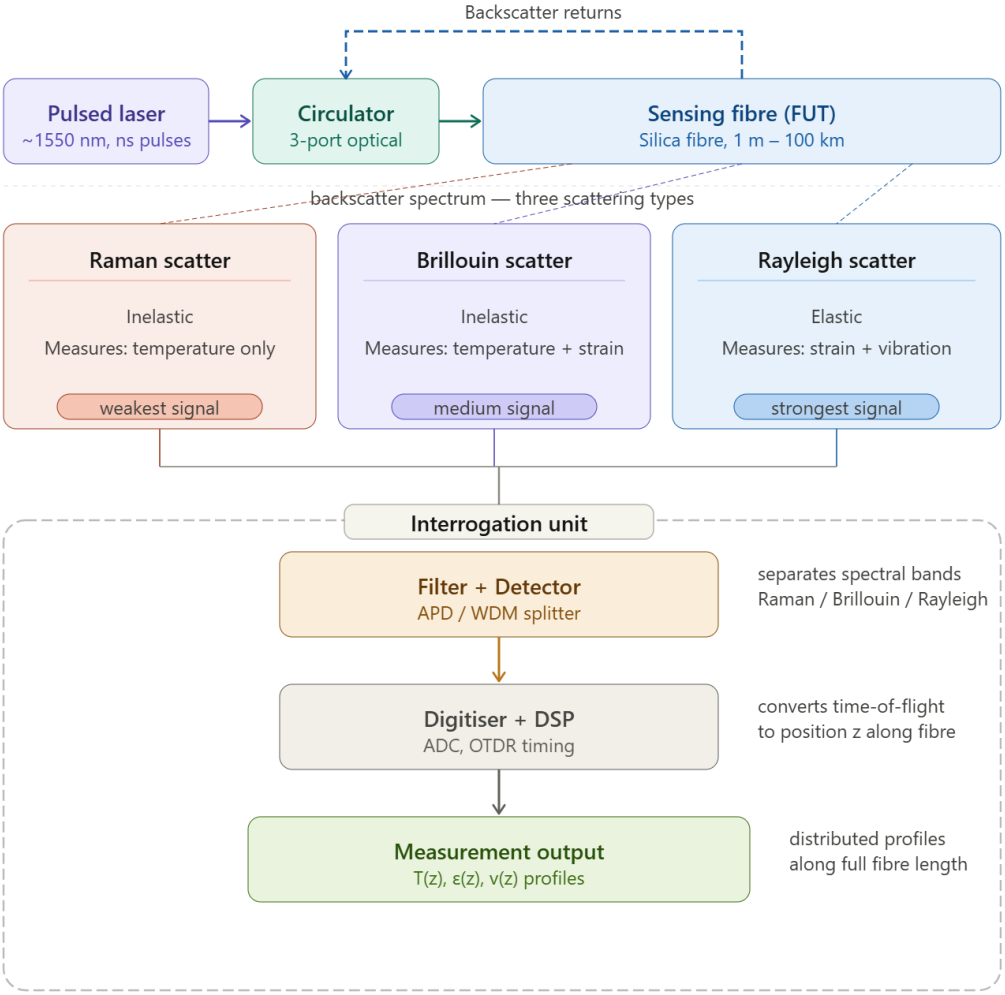

Figure 1. Distributed Fiber Optic Sensing architecture (OTDR - type)

Figure 1 shows the operating principle of a distributed fiber-optic sensing system (DOFS). The pulsed laser directs the probe pulses to the sensing fiber via the optical circulator. In the following stage, the scattered light from all locations of the fiber comes back through the circulator to the photodetection chain. There can be three different forms of scattering inside the fiber. The information on local temperature is contained in the

scattered light in case of Raman scattering. This phenomenon is commonly exploited for the purpose of distributed temperature sensing (DTS). The Brillouin scattering generates the frequency shift, which is dependent on both the temperature and mechanical strain. This property is typically employed in DTS and distributed strain sensing (DSS) applications. The scattered light has the same frequency as the initial one in case of Rayleigh scattering. This phenomenon is dependent on the vibration and strain in the fiber; hence, it can be the basis for the distributed acoustic sensing (DAS) systems. All scattered signals go back through the fiber and are then directed via the circulator to the interrogation unit. In the interrogation unit, a Wavelength Division Multiplexor (WDM) together with avalanche photodiodes (APD) separates the scattered channels from each other. Then, using Optical Time Domain Reflectometer (OTDR) technique and through the use of digitizers and digital signal processors (DSP), the scattered signals are converted into positions along the fiber length according to the arrival time of each scattered signal pulse. The final output is the measured physical quantity, including temperature T(z), strain ε(z), or vibration velocity v(z) which are distributed continuously along the entire fiber length.

As an optical pulse enters the fiber-optic cable made of silica, there is continuous scattering of a small portion of light to the backward direction due to three different physical phenomena. The spectral analysis of backscattered light depicted in figure 2 shows that there are five different peaks on either side of pump laser frequency ν_o, and each peak represents different information regarding the physical condition of the fiber at the location of scattering. The ratios of the amplitudes of the three types of scattering correspond to the ratios of their intrinsic cross-sections: Rayleigh scattering has the most intense, Brillouin scattering has an intermediate, and Raman scattering has the smallest cross-section. These ratios define the system specifications for distributed fiber optic sensors, such as the level of sensitivity of the photodetectors, power of the laser source, pulse width, and averaging scheme of the signals.

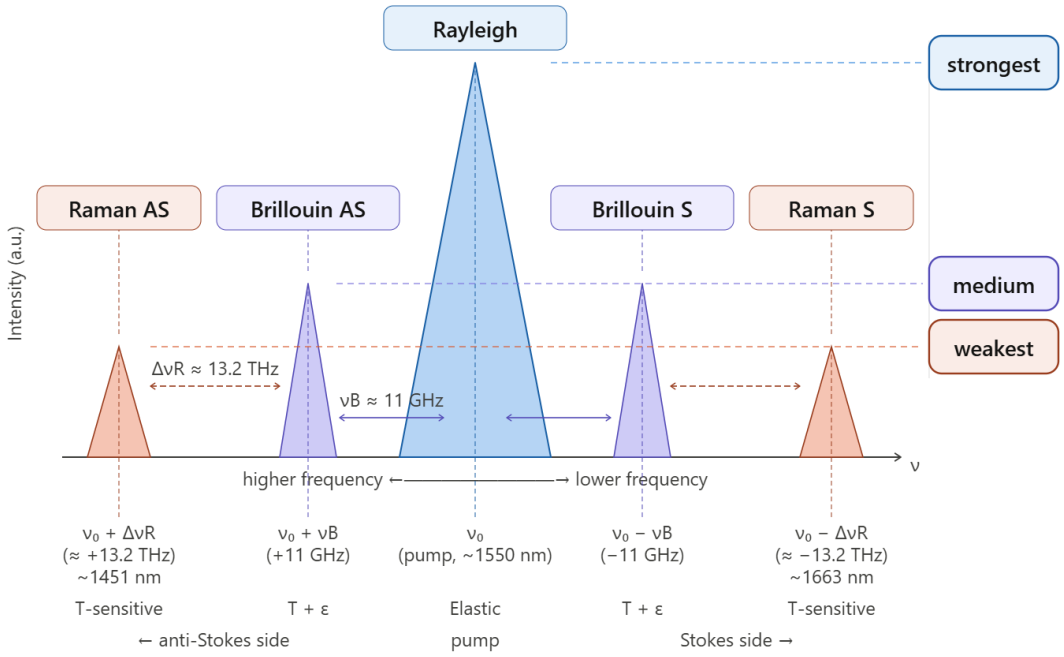

Figure 2. Backscatter Spectrum in the Fiber Optical Sensing

Rayleigh scattering lies at the heart of the backscatter spectrum, with the scattering taking place exactly at the pump wavelength ν_o without any shift in frequency. As there is no exchange of energy between the photon and the scattering medium, the backscattered signal has the same wavelength as that of the incoming signal, typically around 1550 *nm* in case of telecom fibers. Rayleigh backscatter generates the highest amplitude signal and forms the physical foundation of Phase-Sensitive Optical Time-Domain Reflectometry (Φ-OTDR) and Distributed Acoustic Sensing (DAS) technology, where the external disturbance alters the phase of the backscattered signal.

Brillouin scattering takes the form of two symmetrical peaks, separated by about *±11 GHz* from the pump signal, with the anti-Stokes signal at the frequency $\nu_o + \nu B$ and the Stokes signal at the frequency $\nu_o - \nu B$. The physical mechanism of this inelastic type of scattering occurs via parametric interaction between the propagating optical signal and the acoustic phonon waves induced in the core of the fiber due to thermal effects. The energy gap between the scattered photons and the incident radiation is called the Brillouin frequency shift (BFS). It has a well-understood linear relationship with both

local temperature and longitudinal strain in the fiber. Therefore, Brillouin-based distributed sensing schemes including Brillouin optical time-domain analysis (BOTDA) and Brillouin optical time-domain reflectometry (BOTDR) allow for simultaneous or independent sensing of temperature and strain distributions along the entire length of the fiber. The Brillouin scattering is relatively weak but detectable enough to sense up to *100+ km* of fiber distance.

The furthest two peaks in the spectrum correspond to the Raman scattering effect which takes place at offsets from the pump of *±13.2 THz* resulting in wavelength peaks of around *1451 nm* for the anti-Stokes component and *1663 nm* for the Stokes component in silica fiber that is excited at a wavelength of *1550 nm*. Inelastic Raman scattering is based on the photon interaction with the molecular vibrational modes in silica glass structure. The intensity of the anti-Stokes Raman scattering process is highly temperature dependent since the molecular phonons involved in this process must be pre-excited by the thermal energy following the Bose-Einstein distribution law. The Stokes Raman scattering intensity is relatively less dependent on the temperature since this effect is based on the phonon creation rather than absorption. Distributed temperature sensing (DTS) systems utilize the ratio between the anti-Stokes and Stokes intensities to determine the temperature distribution that does not depend on any mechanical strain and is pure temperature based. The anti-Stokes Raman backscatter signal is the least intense signal compared to the other two signals requiring higher optical power pulses and longer integration times to provide good enough signal-to-noise ratios.

The foundation of all distributed sensing is the mapping of backscatter arrival time to fiber position (Li & Zhang, 2022, p. 2). For a pulse of refractive-index-group-velocity

$$v_g = c/n_g: \qquad z = \frac{c \cdot t}{2n_g} \tag{1}$$

where z is the distance from the fiber input to the scattering location, c is the speed of light in vacuum, t is the round-trip travel time of the backscattered signal, and $n_g$is the group refractive index (*~1.468* for standard single-mode fiber at 1550 nm). The spatial resolution of an OTDR is equal to half the length of the probing pulse which should be considered a lower bound to the resolution, since the actual resolution of a DOFS also depends on factors such as the signal-to-noise ratio of the measurement.
The spatial resolution Δz associated with a pulse of duration τ_p is therefore:

$$\Delta z = \frac{c \cdot \tau_p}{2 n_g} \tag{2}$$

A 10 *ns* pulse gives $\Delta z \approx 1\,\text{m}$, while a 1 *ns* pulse gives ~10 cm, but at the cost of proportionally less pulse energy and thus lower SNR.

1.3 Research questions and objectives

The complexity in the choice of various types of sensors, as well as the absence of unified classification framework, which make sense of classifying such devices, poses a necessity to conduct a systematic study of the issue. In this regard, the thesis is based on the three principal research questions that cover different aspects of the topic, ranging from theoretical foundations to practical applications. The two first questions refer to the definition of criteria and classification of the optical sensing devices according to these criteria. The third question focuses on the analysis of collected data during the sensing process in a specific application context.

RQ1: What are the core considerations that need to be taken into account in classifying advanced optical sensing technologies?
RQ2: How can advanced optical sensing systems with their complicated technology be classified and evaluated through the identification of the most important parameters?
RQ3: How is the collected information of the optical sensing of a seabed sediment heat system utilized to get meaningful information?

In order to answer the research questions, the following research objectives have been defined:

O1: To establish a multi-dimensional classification scheme for advanced optical sensing devices.

O2: To study the seabed sediment data collected at Suvilahti, Vaasa, Finland, including the study of temperature variation on heat collection branches over different seasons and years.

1.4 Structure of the thesis

The thesis comprises five chapters. In the first chapter, the domain of optical sensing is described, followed by an introduction to the basics of fiber optic sensing and its three different backscattering mechanisms: Raman, Brillouin, and Rayleigh backscattering. At the same time, three research questions and two objectives of the study are presented. Chapter two provides an overview of the existing scientific literature on the classification of optical sensing systems and seabed sediment temperature measurement technologies. The gaps identified in the literature motivate the creation of the taxonomy developed in this thesis. Chapter three describes the main contribution made in this thesis, which is the creation of a four-dimensional taxonomy of optical sensing systems based on signal encoding principles, light matter interactions, physical structure of the sensors, and applications domains. The fourth chapter provides an analysis of the practical use of Raman-backscatter distributed temperature sensing technology in the Suvilahti seabed sediment heat system in Vaasa, Finland, through which temperature measurements are performed in time and space in two heat collection channels leading to the detection of four thermal regions. Finally, the fifth chapter concludes the thesis and suggests further research based on both theoretical and practical contributions.

2 Literature review

There are many different approaches towards the classification and taxonomy of optical sensors. It is clear from academic research that it is impossible to come up with just one axis for the categorization of such sensors, instead the survey always incorporates different aspects into the taxonomy process. The following section expresses how each work categorizes various optical sensing technologies from different perspectives.

2.1 Optical sensing technologies classification

An applicable classification is offered by (Meng et al., 2026) who review optical sensor applications in water, atmospheric, and soil environmental monitoring. They organize optical sensors by sensing principle into five primary types: absorption spectroscopy-based sensors; luminescence spectroscopy-based sensors; light scattering-based sensors; surface plasmon resonance (SPR) sensors; and by application in water, atmosphere, and soil. In the same way with a broad scope (Sabri et al., 2013) present a basic practical taxonomy in which fiber optic sensors are classified by the optical modulation and in the second step by the relationship between the sensing element and the optical fiber itself, distinguishing between intrinsic fiber optic sensors (IFOS) and extrinsic fiber optic sensors (EFOS). A further taxonomy organizes sensor types into seven distinct categories including chemical sensors, temperature sensors (noted as the largest commercially available class), strain sensors based on FBG technology, biomedical sensors, electrical and magnetic sensors, rotation sensors, and pressure sensors. Large scale applications extend to medical, energy, civil infrastructure, and transportation domains.

A more detailed structural taxonomy is presented in (Wadi Harun, 2025) where in the optical fiber sensors chapter, they categorize sensors into eight distinct types by their operating principle: fiber Bragg grating (FBG) sensors, which use UV-induced periodic refractive index modulation; interferometric sensors, further subdivided into Fabry-Perot interferometers, Mach-Zehnder interferometers, and Michelson interferometers; chemical and biosensors, categorized into four subclasses including enzyme optical

biosensors, whole-cell optical biosensors, immunoassay optical biosensors, and nucleic acid optical biosensors; intensity-based sensors; distributed temperature sensors (DTS) using OTDR-based Raman backscattering; distributed strain sensors (DSS); current and magnetic field sensors employing the Faraday effect or magnetic fluid materials; and displacement and position sensors using interferometry, wavelength modulation, or reflective intensity modulation. Honina, Kazanskiy, and Butt present a configuration-based taxonomy covering photonic crystal fiber (PCF)-based sensors, D-shaped fiber-based sensors, S-shaped fiber-based sensors, U-shaped fiber-based sensors, plastic optical fiber (POF)-based sensors, and fiber Bragg grating (FBG)-based sensors (Khonina et al., 2023). In addition, they classify sensing mechanisms into intensity-based, phase-based, wavelength-based, and polarization-based modulation, and distinguish intrinsic from extrinsic sensor placements.

A detailed categorization of tapered optical fibers is provided by Taha et al.(2021). Eight different categories of tapered optical fibers are proposed according to configuration and operational principles, including: FBG-based tapers ((which further classified as hybrid S-Taper, cascaded S-Taper, Fabry-Perot, and long tapered fiber); long-period fiber grating (LPFG)-based tapers, Mach-Zehnder interferometer (MZI)-based tapers (which are divided based on their cavity construction as follows single cavity, double air cavities, single air cavity, and single air cavity); photonic crystal fiber (PCF)-based tapers; surface plasmon resonance (SPR)-based tapers; multi-taper devices; fiber loop ring-down (FLRD) technology; and optical tweezers. Four different factors that affect the performance of these categories have been described, namely taper length, sensitivity, refractive index/wavelength range, and waist diameter. Moreover, individual challenges for each category have been proposed separately, making these sensors suitable for use in biological/chemical sensing, medicine, environment sensing, and industry processes.

A review of distributed fiber-optic sensing technology for the oil and gas sector is provided by (Ashry et al., 2022). The main criteria in which the classification can be carried out is the physical phenomenon that is exploited; namely: distributed acoustic

sensing (DAS), using the principle of Rayleigh scattering; distributed temperature sensing (DTS), using the principle of Raman scattering; and distributed strain sensing (DSS), using the principle of Brillouin scattering. DAS is further classified by operational modality into direct detection (differential intensity) and phase-sensitive detection schemes including interferometric recovery, coherent detection, dual-pulse, and chirped-pulse approaches, and also classified by fiber type into standard SMF-based systems versus engineered or specialty fiber variants with enhanced Rayleigh scattering. Further research in the distributed sensing field has been provided by Ding and et al., who classify Optical Frequency Domain Reflectometry (OFDR) systems and compare those with Optical Time Domain Reflectometry (OTDR) (Ding et al., 2023). Within OFDR systems, the review classifies sensing modalities by measured parameters including strain sensing, temperature sensing, vibration sensing, and shape sensing, and distinguishes single-mode fiber (SMF) and polarization-maintaining fiber (PMF).

The sensitivity enhancement dimension of distributed acoustic sensing specifically is classified into two complementary approaches: enhancement of Rayleigh scattering intensity through modification of refractive index uniformity in the fiber core, and enhancement of optical path modulation through structural and material design of the fiber coating and cable jacket (Xiao et al., 2022). The paper identifies seven cable structure types identified and ranked by acoustic sensitivity and mechanical strength: tight buffer fiber; plastic loose tube cable with gel; ribbon fiber in plastic or metal tube; fibers dispersed in solid polymer sheath; armored plastic loose tube cable with gel; fibers twisted with aramid; and metal loose tube cable with gel. The field of polarization-based optical fiber sensing is addressed by Pellegrini and et al. (2024). Their taxonomy differentiates state-of-polarization (SOP) from DAS by hardware requirements, sensing principle, cost, operational range, and event localization capability. A further classification organizes detection hardware into dedicated polarimeters, polarization beam splitters, and commercial coherent receivers. Hydrogen-specific fiber optic sensing is also considered as a specialized domain (Wang et al., 2026). They develop a multi-level classification based on sensing principle, material, architecture, and application context.

The standard scattering-mechanisms, including Rayleigh-based DAS, Raman-based DTS, Brillouin-based DTS/DSS, and FBG-based wavelength demodulation are compared in a systematic table by detection range, spatial resolution, accuracy, and strain sensitivity. Point fiber optic hydrogen sensors are also classified into four architectures: end-face sensors detecting reflectivity changes of hydrogen-sensitive films; grating-type sensors using FBG or LPG with sensitive coatings; interferometric sensors based on Mach-Zehnder, Fabry-Perot, or microinterferometer cavities; and evanescent-field sensors using tapered, D-shaped, or side-polished fibers. Application fields are further classified by deployment context into hydrogen storage tanks, liquid hydrogen storage, hydrogen refueling stations, fuel cell systems, onboard hydrogen cylinders, nuclear facilities, and aerospace applications.

Optical spectroscopy techniques are classified by technology type and by functional purpose into four categories (Rashed et al., 2025). Ultraviolet-visible spectroscopy based on electronic transitions in the UV-Vis region; photoluminescence (PL) spectroscopy, including three-dimensional fluorescence variants; near-infrared (NIR) spectroscopy operating from 4000 to 12000 cm^{-1} for dissolved fault gas detection; and Fourier Transform Infrared (FTIR) spectroscopy in the range of 400 to 4000 cm^{-1} for direct molecular fingerprint identification. The presented classification distinguishes condition assessment (dissolved decay products, dielectric dissipation factor, breakdown voltage, moisture content, interfacial tension, acidity, and color index) from fault diagnosis (fault types as defined by IEC and IEEE standards through characteristic spectral features). Optical sensing in the context of smart road transportation infrastructure is organized across three axes: sensor type, physical parameter measured, and integration with emerging digital technologies (Senkans et al., 2026). The sensor type sub-category distinguishes quasi-distributed FBG sensors from three classes of fully distributed fiber-optical sensors (Raman distributed sensing, Brillouin distributed sensing, and Rayleigh distributed sensing). Another different parallel taxonomy of classical electrical sensors including resistive strain gauges, vibrating wire strain gauges, piezoelectric transducers, LVDTs, accelerometers, and electrical temperature sensors is presented. The physical

parameter taxonomy maps sensor technologies to measurable quantities: temperature, strain, vibration, pressure, displacement and tilt, and humidity. Finally, a comparative matrix evaluates all technologies across measured parameters, resolution, accuracy, robustness, technology readiness level, and cost.

Gorji et al. (Gorji et al., 2024) review optical sensing in indoor farming and controlled environment in a systematic way following PRISMA 2020 guidelines. Their technology taxonomy classifies optical sensing systems into five types: UV-VIS spectroscopy (200–800 nm) primarily used for macronutrient quantification in liquid fertilizers and non-destructive quality evaluation; visible and near-infrared spectroscopy (VIS-NIR), including NIRS and the Aquaphotomics sub-discipline, used for nutrient content, moisture detection, and quality assessment; mid-infrared spectroscopy (MIR) for chemical fingerprinting; Raman spectroscopy for disease diagnosis, stress detection, and nutritional assessment; and hyperspectral imaging (HSI), which integrates spectroscopy and imaging across the UV to thermal infrared range. Application domains within indoor farming are also classified into precision agriculture (irrigation and fertilizer management), disease and deficiency detection, and quality assessment. The integration of machine learning algorithms with optical sensing systems is presented as a cross-cutting classification axis, with algorithm types ranging from PLS and PCA to convolutional neural networks and recurrent neural networks.

Zhu et al. (2026) present their taxonomic work on acoustic technologies with respect to noise pollution in underwater environments. The authors discuss offshore wind farm noise and categorize underwater acoustic monitoring systems architecture according to four deployment methods, including: buoy-based real-time passive acoustic monitoring (PAM) nodes using both hydrophones and telemetry for real-time data transmission; autonomous seabed archival recorders enabling long-term, low-self-noise baseline recording; cabled hydrophone arrays with data acquisition and signal processing (DAQ/DSP) pipelines offering constant power and high-bandwidth real-time data; and fiber-optic distributed acoustic sensing (DAS), which allows for continuous spatial

coverage in kilometers through existing fiber-optic cable infrastructure. Furthermore, the authors classify acoustic sources according to their lifecycle phase, i.e., preparation, construction, mechanical vibration at the time of operation (from gearbox and generator), and decommissioning (underwater cutting and blasting). The paper's strength is its interdisciplinary taxonomy, specifically in relation to acoustic monitoring technology, biological effects, and governance structure.

According to figure 3, the reviewed literature reveals a convergence on the sensing mechanism and scattering principle as the primary classification factor, whether for broadband optical sensors organized by absorption, emission, and scattering phenomena, or for fiber sensors classified by Rayleigh, Brillouin, and Raman backscattering. Structural configurations such as FBG, tapered, D-shaped, U-shaped, photonic crystal, plastic, and distributed fiber geometries, emerge as the most common secondary axis. Application domain is the next criteria mostly used for classification. Performance -based taxonomies, including spatial resolution, sensing range, sensitivity in physical units, and technology readiness level, appear increasingly in more recent works.

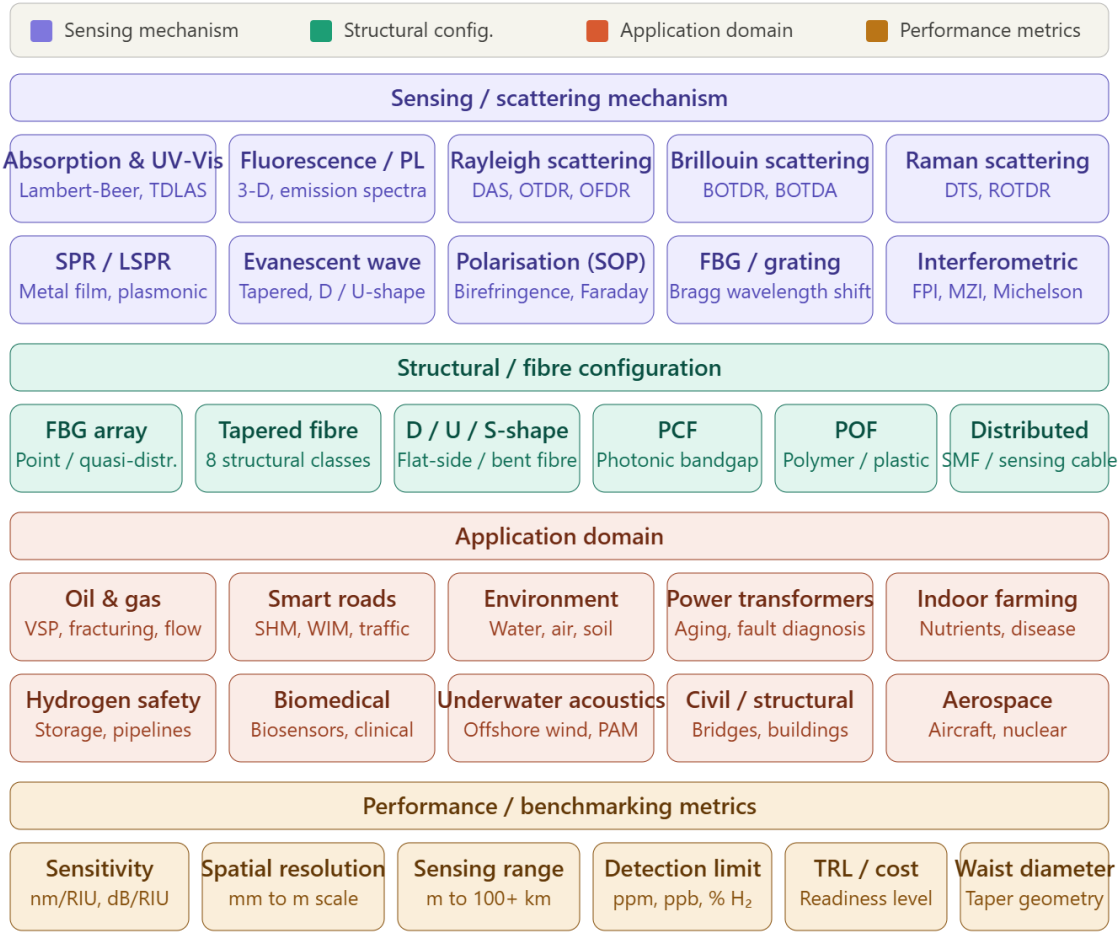

Figure 3. Taxonomy in literature

2.2. Technologies for Measuring Temperature in Sea Sediment Layers

Pelaez Quiñones et al.(2023) utilize fiber-optic Distributed Acoustic Sensing (DAS) technology as a high-resolution thermometry tool along the seafloor. They utilize existing submarine telecommunication cables, which span tens of kilometers along the seafloor, as dense arrays of temperature anomaly sensors without requiring any new hardware deployment. By using low-frequency DAS (LF-DAS) alongside Distributed Strain and Temperature Sensing (DSTS) on parallel fibers, they are able to detect thermal anomalies at the millikelvin level. Gutscher et al. (2025) take a similar approach to seafloor thermal monitoring by using Brillouin-based Distributed Temperature Sensing (DTS). Unlike the DAS approach, which measures temperature anomalies, Brillouin-

based DTS tracks absolute temperature along the fiber by analyzing shifts in the Brillouin frequency of backscattered light. The study recorded measurements every three to six months over a three-year period from 2022 to 2025, where it detected clear seasonal temperature cycles on the seafloor and captured a rapid marine heatwave between 2022 and 2024, in which temperatures rose by approximately 1.5°C.

Distributed Temperature Sensing (DTS) method is applied to detect changes in sediment overburden above buried seafloor infrastructure (Rui et al., 2019). The concept relies on burying a fiber-optic cable beneath the seabed and using an electrical heat source to generate a controlled thermal pulse into the surrounding sediment. A Brillouin Optical Time Domain Analysis (BOTDA) system then monitors how the temperature field evolves in space and time along the cable. The system achieves spatial resolution of ±0.5 m with a temperature sensitivity of 0.3 $^{\circ}C$ and a temporal resolution of less than 5 minutes. Zhao et al. (2025) provide an overview of how different backscatter-based and point-sensing technologies are being applied to ocean observation challenges including seafloor and sediment temperature monitoring. The paper organizes optical sensing approaches by their physical principle: Rayleigh backscatter-based DAS for seismic and acoustic monitoring; Raman backscatter-based DTS for continuous temperature profiling along cables and vertical sections in the water column and near the seafloor; and Brillouin backscatter-based systems for simultaneous temperature and strain measurement in seafloor geological applications. The application of each technology is discussed such as the use of DTS for studying hydrothermal activity, and the use of Brillouin sensing for cable health monitoring in sediment-bearing environments. The review also highlights how existing submarine telecommunications infrastructure, including cables that are buried in seafloor sediment, is increasingly being implemented as a distributed sensing network.

Liang et al. (2022) conduct an extensive survey about the application of optical fiber sensor technologies in measuring temperature, salinity, and pressure in the ocean as

well as in sediment layers. In another study, Zhao et al. (2025) develop an all-fiber expendable bathythermograph (AOF-XBT), which uses two cascaded Fiber Bragg Gratings (FBGs) to simultaneously measure temperature and depth with a accuracy of 0.01℃ and a measurement error of ±0.02℃. The review also covers Mach-Zehnder interferometers (MZI), Fabry-Pérot interferometers (FPI), and Surface Plasmon Resonance (SPR) configurations, with analysis of their performance for open-ocean as well as seabed measurements. Zhuang et al. (2024) explore the use of optical fiber sensors in situ for detecting environmental variables in the marine environment. They consider various interferometric configurations, including Fabry-Pérot interferometers (FPI), Mach-Zehnder interferometers (MZI), and polarization-maintaining fibers. The review also addresses practical challenges for sediment deployment, including the encapsulation and packaging of fiber sensors to protect them from the mechanical stresses of sediment insertion and the corrosive effects of pore water chemistry.

Table 1. Comparative overview of key methods across selected papers

AUTHOR	TECHNOLOGY	INSTRUMENT	SENSING PRINCIPLE	PRECISION
Pelaez et al., 2023	DAS	Fiber-optic telecom cable	Rayleigh backscatter / thermo-optic effect	~ 0.001°C
Gutscher et al., 2025	Brillouin DTS	Submarine telecom cables	Brillouin frequency shift	0.1–0.3°C
Rui et al., 2019	Active DTS	Buried fiber-optic cable	BOTDA	±0.3°C
Li et al., 2022	FBG (AOF-XBT)	Cascaded FBG	Bragg wavelength shift	±0.02°C
Liu et al., 2025	DAS · DTS · FBG	Submarine cables + point FBG sensors	Multiple optical backscatter	Varies by mode
Zhuang et al., 2024	FPI · MZI · FBG	point-based sensing	Interferometric spectral shift	< 0.1°C

Table 1 presents a structured comparison of key studies that applied optical sensing technologies for measuring temperature in sea sediment and seafloor environments.

3 Taxonomy of Optical Sensing Technologies

The optical sensing technologies include various ranges of physical principles, hardware configurations, measurable quantities, and application contexts, and there is no single criterion for classification. The taxonomy presented in this thesis was developed based on the six classification factors which provide comprehensive knowledge regarding operation principle of the sensor, its construction, type of quantity being measured and its location in a measurement process. The first factor is interaction mechanism, that defines what happens to light when it encounters matter. The sensing geometry is the second factor characterizing geometric configuration of light traveling through a device in terms of light transmitting, reflecting and wave-guiding principles. The third factor is signal detection method, which expresses how useful information is extracted from the optical signal. Spatial sensing mode is the fourth factor, distinguishing between point sensors that measure at a single location, distributed sensors that profile a measurand along a long path. The fifth factor, the target phenomenon, identifies what is being measured like physical characteristics, chemical species or biological entities. The final one is the spectral region of operation, which refers to the part of the electromagnetic spectrum that is used.

As shown in figure 4, the multi-layered classification is divided into four major groups, which all depict a certain characteristic of the optical sensors. Category I classifies sensors based on how they modulate the optical signals. Category II analyses how light interacts with material. Category III covers the physical platforms and system architectures, and category IV explains the real-world application domains.

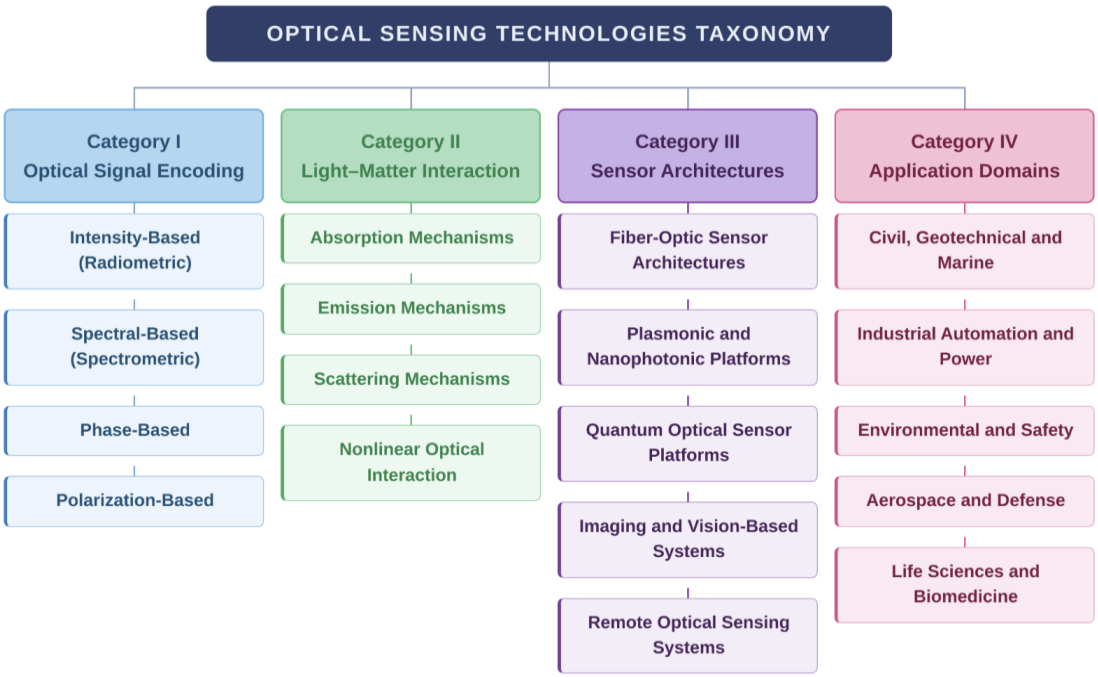

Figure 4. Optical Sensing Taxonomy

3.1. Category I: Optical Signal Encoding

Category I classifies optical sensing technologies according to the physical principle that light is encoded and read out by the detector to extract useful information. This is the foundational factor for analyzing optical sensors. As shown in figure 5, the group is divided into four sub-categories: Intensity-Based, Spectral-Based, Phase-Based, and Polarization-Based sensing.

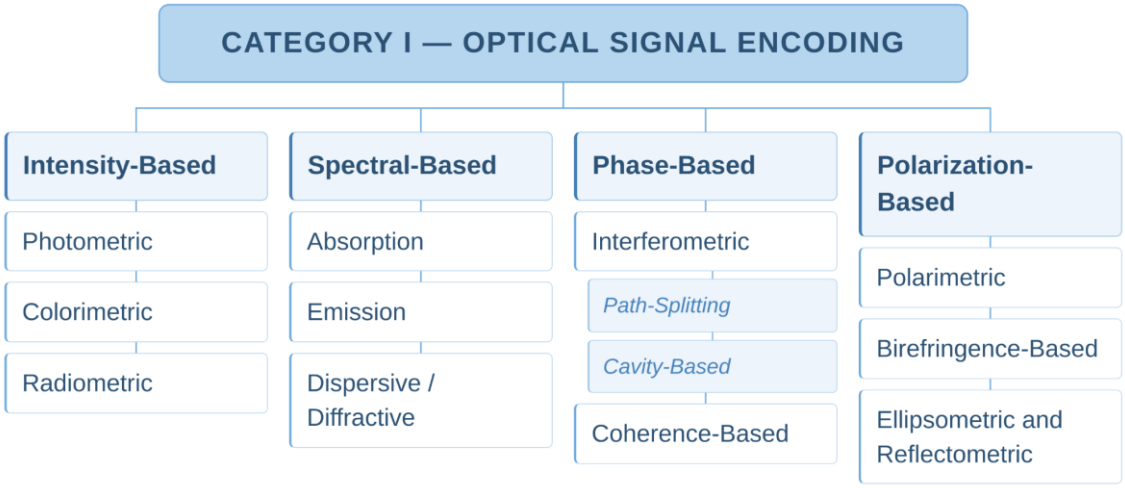

Figure 5. Category I: Optical Signal Encoding

3.1.1 Intensity-Based Sensing

Intensity-based methods are the oldest and simplest way of encoding optical signals, relying on the modulation of the radiation's amplitude. In this method, the brightness (the optical power) is changed after hitting the matter, and this change, which can be related to the material's properties based on the Beer-Lambert law, is interpreted as a measurement signal. The three sub-categories of Intensity-based sensing are Radiometric, Photometric, and Colorimetric sensing. In Radiometric sensing the total optical intensity is measured, and wavelength components are not considered. It is the broadest form of optical intensity measurement and a foundation for other two sub-categories. Optical power meters, Turbidity sensors, and Fiber-optic loss-based sensors are common technologies using Radiometric sensing. Photometric sensing concentrates exclusively on the visible wavelength range, typically between 400 and 700 nm. In this sensing method, the total optical intensity within this visible range is measured and wavelength components outside this range are not considered. Changes in intensity usually occur due to absorption or scattering (Khonina et al., 2023, p. 3). Colorimetric sensing uses the specific wavelength composition of light to identify and quantify substances. It is essentially a simple form of spectroscopy in which each substance has

its own chemical properties that produce visible color changes detectable by the sensor (Fedenko et al., 2017, p. 15). This method is widely used in chemical and biochemical sensing such as pH indicators and test strips, Paper-based chemical sensors, and Optical biosensors.

3.1.2 Spectral-Based Sensing (Spectrometric)

Spectral-based sensing focuses on the interaction of the different wavelengths of light with matter. Detailed information about material composition can be extracted by analyzing how different wavelengths are absorbed, emitted, or dispersed. In the absorption method, for example, the Beer–Lambert law, can be used to assess the chemical properties of the matter based on the attenuation in specific spectral bands. Infrared spectroscopy (IR, FTIR), visible–near infrared (VIS–NIR) spectroscopy, and non-dispersive infrared (NDIR) gas sensors are the most common applications of absorption method (Griffiths & de HASETH, n.d., p. 12). In the emission-based sensing, the molecules of a matter are excited by the incident light and then emit different wavelengths, which can be analyzed to understand the chemical bonding and components of different materials. Fluorescence spectroscopy, Quantum-dot and carbon-dot sensors, and Optical biosensors all utilize emission-based sensing. In dispersive and diffractive readout systems different gratings and prisms are used to separate light into its spectral components. Application of Fiber Bragg Grating (FBG) in hyperspectral imaging systems implementation is a dominant example of this sub-category.

3.1.3 Phase-Based Sensing

Phase-based sensing utilizes the coherent wave nature of light and encodes information regarding the timing of light waves instead of amplitude or spectral content. This feature leads to very high sensitivity and immunity to amplitude noise. Phase-based sensing is divided into two main categories: interferometric sensing and coherence-based sensing.

Interferometric sensing involves positioning of two or more coherent light to produce interference patterns, which are highly sensitive to phase changes. These interference patterns are created by path-splitting interferometry or cavity-based interferometry. In the path-splitting interferometry a coherent light beam is divided into two or more separate optical paths, usually one as a sensing arm and another as a reference arm. By recombining them, the phase differences which are accumulated along the paths produce interference patterns that are highly sensitive to changes in optical path length or refractive index. Mach–Zehnder interferometers and Michelson interferometers benefit from path-splitting method. Cavity-based interferometry relies on multiple reflections of light within an optical cavity, such as a Fabry–Pérot structure. In this method, resonance conditions strengthen phase changes and lead to precise detection of small variations in distance, refractive index, or environmental parameters.

Coherence-based sensing utilizes the temporal or spatial coherence properties of light rather than a fixed interferometric path. The information about a sample is typically extracted by analyzing interference signals that depend on the coherence length. One of the main examples of this method is Optical Coherence Tomography (OCT). This technique is based on low-coherence interferometry (which uses light with a short coherence length) and creates cross-sectional images of a sample. It works by scanning different depths and detecting reflected light, and due to its high precision, this technique is widely used in biological tissues imaging without physically cutting them and also in non-destructive inspection of materials (Ding et al., 2018, p. 2).

3.1.4 Polarization-Based Sensing

Polarization-based sensing extracts information based on the orientation of the electric field vector of light instead of its amplitude, frequency, or phase. When optical sensors are affected by an external influence like mechanical stress, magnetic field, electric field, or change in refractive index, the polarization state of the propagating light is changed. This rotation of the light can be detected with high precision using polarimetric instrumentation. Polarization-based sensing is divided into three main categories:

Polarimetric sensing, Birefringence-Based Sensing, and Ellipsometric and Reflectometric Sensing. Polarimetric sensing deals with determining the total alteration in the state of polarization of light following interaction with the sample, including any alteration in its orientation or ellipticity. Polarimetric sensing is extensively used for sensing through the application of Faraday Effect, which uses magnetic fields in a power conductor to cause an angular change in the light's plane of polarization. Distributed polarimetric optical frequency domain reflectometry (P-OFDR) is a dominant technology that has been used for non-invasive monitoring of high-voltage power lines and substations with millimeter spatial resolution (Palmieri et al., 2015, p. 2).

Birefringence-based sensing relies on materials that have different refractive indices for different polarization directions. When light passes through such materials, it splits into two components that travel at different speeds, creating a phase difference that can be used to measure quantities like strain, stress, or temperature. Fiber-optic gyroscopes based on the Sagnac effect, that are mostly implemented in inertial navigation systems for aircraft, submarines, and autonomous vehicles (Sabri et al., 2013, p. 4), utilize this sensing technology. Ellipsometric and reflectometric sensing focuses on how polarization changes when light reflects from the surface. By analyzing these changes, it is possible to obtain very precise information about thin films, surface layers, and material interfaces.

3.2. Category II: Light-matter interaction

This category classifies optical sensing techniques based on the physical interaction between light and matter. When light encounters a material, it can be absorbed, emitted, scattered, or undergo nonlinear interactions. These processes determine how information about the material is encoded in the optical signal. As illustrated in figure 6, this category is organized into four main sub-categories: Absorption, Emission, Scattering, and Nonlinear Optical Interaction, each of which includes several sensing approaches.

3.2.1 Absorption Mechanisms

Absorption occurs when the light photons are absorbed by a material and their energy transfer to them, typically exciting electrons or molecular vibrations. The amount of absorbed light depends on wavelength and material properties, which is utilized for identification and quantification of different substances. The relationship between absorbance and concentration is given by the Beer-Lambert law, which states that absorbance is proportional to the product of the molar absorptivity, the optical path length, and the analyte concentration (Rashed et al., 2025, p. 5). Broadband absorption and Laser-Based absorption are considered as two main subcategories.

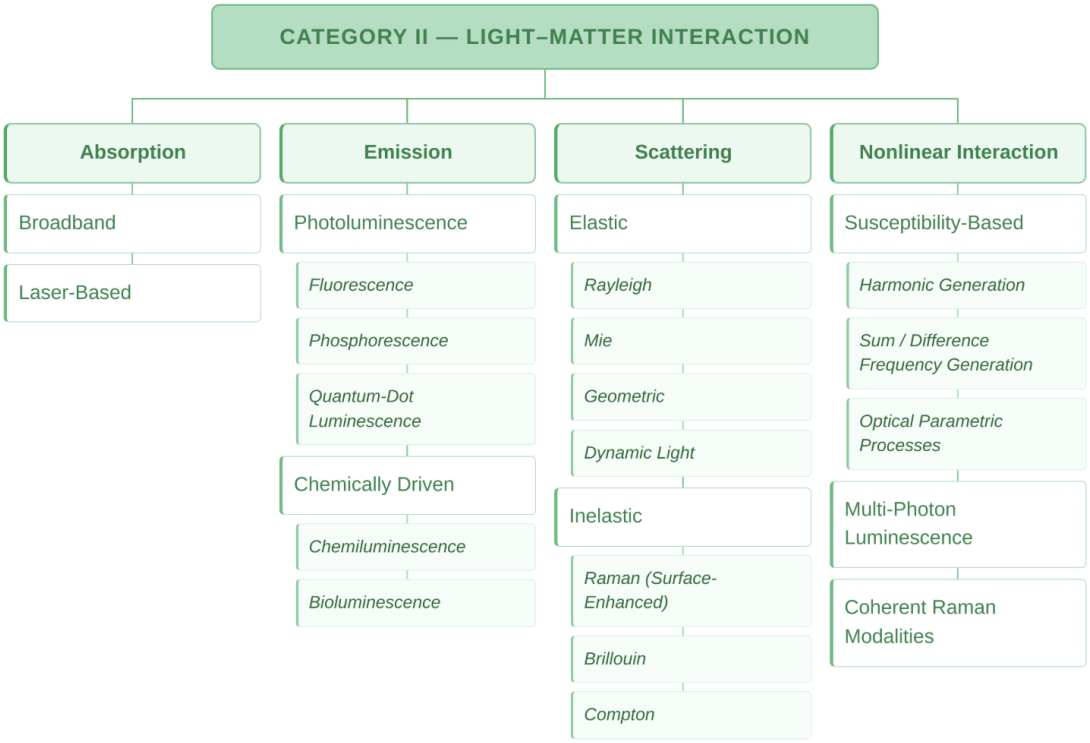

Figure 6. Category II: Light-matter interaction

Broadband absorption uses white light sources with a wide spectral range to measure overall attenuation across multiple wavelengths. This approach is commonly used in general spectroscopy and chemical sensing. On the other hand, Laser-based absorption uses narrowband, coherent light sources to measure absorption at specific wavelengths

with high sensitivity and selectivity. Tunable diode laser absorption spectroscopy (TDLAS), Cavity ring-down spectroscopy (CRDS), and Differential Optical Absorption Spectroscopy (DOAS) are the most famous and fast-growing techniques.

3.2.2 Emission Mechanisms

Emission occurs when a material absorbs light, and after excitation, releases part of this energy as emitted light. The emitted radiation carries spectroscopic information about the electronic or molecular structure of the material. Two main groups relevant for fiber optics sensing in this sub-category are Photoluminescence and Chemically Driven Emission.

Photoluminescence contains all processes (Fluorescence, Phosphorescence, and Quantum-Dot Luminescence) in which a material absorbs a photon and then re-emits light. The fastest and most widely applied method is fluorescence, which occurs when a molecule absorbs UV or visible light and immediately emits at a longer wavelength via a single-state transition. The emission typically happens within nanoseconds and is sensitive to the local chemical environment. Fluorescence, famous for its high sensitivity, reaching parts-per-billion (ppb) or even parts-per-trillion (ppt) levels, is vastly used in a range of biosensors and environmental monitoring tools (Meng et al., 2026b, p. 159). Phosphorescence is an example of fluorescence; however, it is characterized by a delayed emission process owing to the formation of longer-lived excited states. In phosphorescence, the generated luminescence can persist for milliseconds and even longer following the removal of the excitation energy source. The ability to maintain this light makes it possible to employ the phenomenon in time-resolved luminescence sensors. The luminescence of quantum dots emanates from the use of semiconductor nanocrystals that emit light once excited (Loskutova et al., 2025, p. 1). The emission wavelength that varies according to the sizes of the quantum dots allows for fine-tuning of the emitted light's wavelength. The use of quantum dots in sensing and imaging processes is widespread because of their brightness and stability properties. Quantum

dots are increasingly implemented in multiplexed bioassays and in vivo imaging where conventional methods suffer from photobleaching (Khonina et al., 2023, p. 3).

Chemical emission involves the production of light due to a chemical or biochemical reaction instead of optical excitation. This type of light emission is commonly utilized in analytical chemistry and biology without the presence of light energy from outside sources. Chemiluminescence and bioluminescence can be considered the two major subtypes of chemical emission. Chemiluminescence refers to light emission through a chemical reaction that releases energy in the form of photons. In most cases, the intensity of light emitted increases as the concentration of reactants increases. Bioluminescence is a special case of chemiluminescence whereby light is emitted by a biological organism via enzymatic reactions (Loskutova et al., 2025, p. 17). It is commonly used in biomedical sensing and imaging because of its high specificity and low background noise.

3.2.3 Scattering Mechanisms

Scattering occurs when light is redirected in new directions after encountering particles or molecules. It can occur with (Inelastic) or without (Elastic) energy change and provides both physical and chemical information.

In elastic scattering, light is redirected by particles without a change in wavelength. The scattered light maintains the same energy as the incident light, and this process provides information about particle size and structure. Rayleigh scattering relates to the interaction of light with very small variations in density or particles that are much smaller than its wavelength. This causes a small amount of backscatter light toward the source. This effect is used in Distributed Acoustic Sensing (DAS) (Wang et al., 2026, p. 222), where a coherent laser pulse is sent into the fiber and the backscattered Rayleigh light is measured. When vibrations or acoustic events occur, they slightly change the optical path length in the fiber, which consequently alters the phase of the backscattered signal. By detecting these changes, DAS systems can monitor events such as seismic activity,

pipeline disturbances, and other acoustic signals over long distances (Ashry et al., 2022, p. 1407). In Mie scattering, the size of the particles is equal to the wavelength of light and unlike Rayleigh scattering, it is less dependent on wavelength. It is commonly observed in systems such as clouds and aerosols and widely used in particle characterization (Knight et al., 2022, p. 1572). When particles are much larger than the wavelength of light, Geometric scattering will occur and the light behavior can be described using classical optics, including reflection and refraction. Dynamic light scattering, in contrast, measures small changes in scattered light intensity over time due to the motion of particles. The particle size and distribution can be determined by analyzing these fluctuations.

On the other hand, in Inelastic scattering, light exchanges energy with a material, leading to change in wavelength. This process provides detailed information about molecular vibrations and material properties. Raman scattering (Surface-Enhanced) is the most important inelastic process. When a photon interacts with molecular vibrations, it gains or loses a discrete amount of energy. This generates Stokes or anti-Stokes scattered light, that their shifted wavelengths provide a molecular fingerprint (Ashry et al., 2022, p. 1410). The anti-Stokes component of Raman backscatter in optical fibers strongly depends on temperature, and Raman-based Distributed Temperature Sensing (DTS) uses this property to measure temperature continuously along fibers (Ashry et al., 2022, p. 1417). Brillouin scattering results from the interaction of light with thermally driven acoustic waves, which produces a frequency shift, the Brillouin frequency shift (BFS), that is linearly dependent on both temperature and strain. This is the main reason that Brillouin-based distributed sensing is the only technology providing both temperature and strain measurement from a single fiber (Wang et al., 2026, p. 231). The BOTDA (Brillouin Optical Time Domain Analysis) system is the most widely implementation, achieving the high accuracy of temperature and strain (Ashry et al., 2022, p. 1421). Compton scattering occurs when high-energy photons interact with electrons, resulting in a significant change in wavelength. It is primarily relevant in high-energy physics and is less commonly used in optical sensing applications.

3.2.4 Nonlinear interaction

In Nonlinear optical sensing, light interacts with a material at very high intensities, usually produced by pulsed lasers, and the material does not respond in a simple way such as proportional to the light.

Susceptibility-based interaction arises from the situation where the behavior of the material under study depends on the power level of the incident electromagnetic wave. This class of interaction is characterized by the second or third order susceptibility of the material involved, and it normally requires a high-level optical power source (Boyd, 2019, p. 4). Harmonic generation involves the production of additional output at the multiples of the fundamental frequency; examples include second harmonic generation. It is widely used in nonlinear microscopy and frequency conversion (Boyd, 2019, p. 184). Sum and Difference Frequency Generation (SFG and DFG) combine two input beams of different frequencies to generate a third at their sum or difference, and Vibrational Sum Frequency Generation (VSFG) spectroscopy uses this principle to probe molecular orientation and bonding at surfaces (Boyd, 2019, p. 86). In optical parametric processes, energy exchange takes place between interacting light rays in a non-linear medium. Optical parametric processes are capable of producing coherent light across various wavelengths. If multiple photons are absorbed in excitement of a substance at one time, the phenomenon of multi-photon luminescence occurs. Multi-photon luminescence enables deeper imaging within biological tissues because of low scatter (Diaspro et al., 2005, p. 115). In coherent Raman spectroscopy, several laser beams are used to increase the Raman signal for faster and better image acquisition. These techniques have found widespread applications in optical and chemical imaging (Evans & Xie, 2008, p. 884).

3.3 Category III: Sensor Architecture

Category III analyzes optical sensing technologies according to the physical platform and system architecture. This is not about the interaction of light with matter or signal

encoding, but rather the physical structure of the sensor itself and how it is implemented in space. This is the engineering aspect of taxonomy, because architecture determines the sensor's form factor, deployment range, spatial resolution, multiplexing capability, and compatibility with existing infrastructure in real-world applications. As shown in figure 7, Category III includes five sub-categories: Fiber-Optic Sensor Architectures, Plasmonic and Nanophotonic Platforms, Quantum Optical Sensor Platforms, Imaging and Vision-Based Systems, and Remote Optical Sensing Systems.

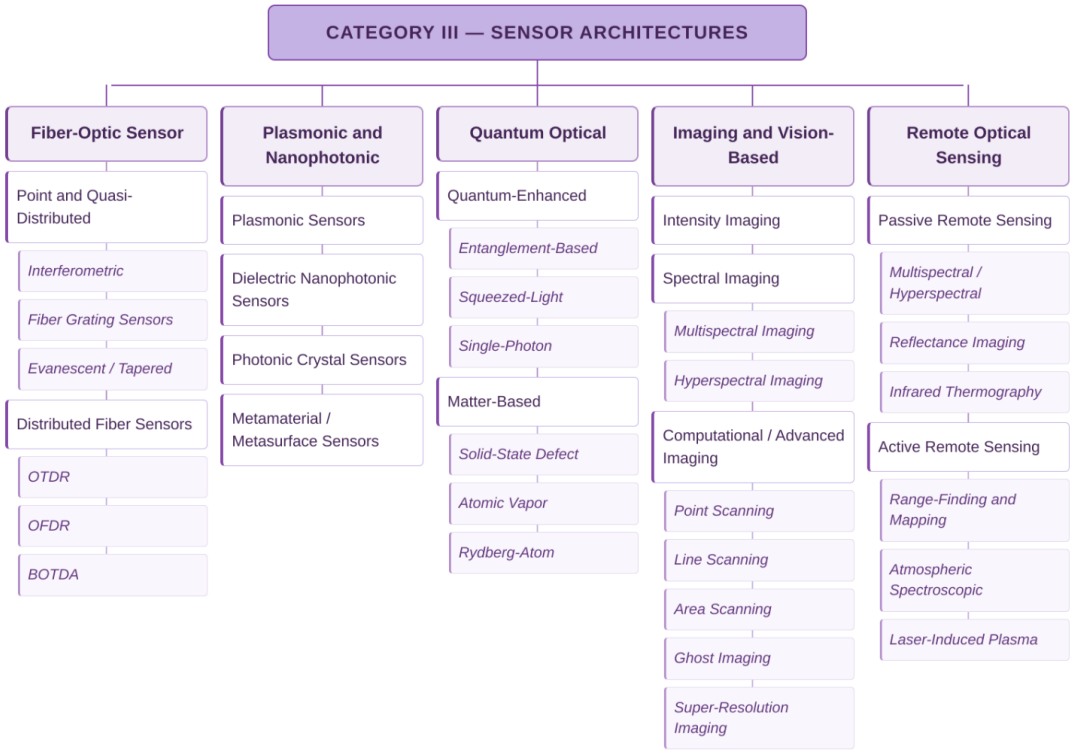

Figure 7. Category III: Sensor Architecture

3.3.1 Fiber-Optic Sensor Architectures

The architecture of fiber optic sensors relies on optical fiber as a material for sensing and also signal transmission medium. This capability enables measurements over long distances with high immunity to electromagnetic interference and resistant to corrosion (Khonina et al., 2023, p. 1). These systems can operate as point, quasi-distributed, or fully distributed sensors depending on how measurements are obtained along the fiber.

Point and quasi-distributed fiber-optic sensors make measurements at one or at discrete locations along the fiber. Three principal architectures can be distinguished in this category. Interferometric fiber sensors split light into two arms, one protected from the environment as a reference, the other used for measurement, and detect the phase difference between them caused by variations in strain or temperature. Mach-Zehnder (MZI) and Fabry-Pérot interferometers (FPI) are the most widely used configurations; MZI-based sensors have been demonstrated for refractive index sensing with a high degree of sensitivity, making them suitable for food safety and chemical process control (Wadi Harun, 2025, p. 45). Fiber Bragg Grating (FBG) sensors are created by making very small, regular changes in the refractive index inside the core of an optical fiber using ultraviolet (UV) light, which causes the fiber to act like a mirror that reflects a specific wavelength of light. When the grating is stretched or heated, the reflected Bragg wavelength shifts accordingly. This shift allows the sensor to measure strain and temperature. FBG arrays are now applied for composite aerospace structures, wind turbine blades, and railway tracks for real-time structural health monitoring (Sabri et al., 2013). Evanescent and tapered fiber sensors decrease the fiber diameter to a few micrometers, so that a fraction of the guided light goes beyond the fiber surface as an evanescent field that interacts directly with the surrounding medium. Any change in the refractive index of that medium such as adsorption of molecules, the presence of a gas, or a change in temperature, modulates the transmitted optical signal (Taha, 2021, p. 3). Tapered fiber SPR sensors are development area which combines evanescent-field coupling with plasmonic resonance to achieve label-free biosensing with sensitivities of over *1600 nm/RIU* in some photonic crystal fiber configurations (Taha, 2021, p. 10).

Distributed fiber sensors measure a physical parameter along the entire length of the fiber. In these sensors, every single point along the cable is converted into a sensor node. The three main implementation technologies are OTDR (Optical Time Domain Reflectometry), OFDR (Optical Frequency Domain Reflectometry), and BOTDA (Brillouin Optical Time Domain Analysis). OTDR method involves laser pulse injection in the fiber followed by recording of the backscattered light as a function of time to determine the

position of changes along the fiber. Phase-sensitive (ϕ-OTDR) version of this technique has been extensively used for vibration detection in DAS systems, such as seismic wave detection, pipelines monitoring, and rail movement tracking within a maximum distance of 150 km (Ding et al., 2018, p. 14). The OFDR technique utilizes a frequency-swept laser rather than pulses, which provides very high resolution (in the sub-millimetre range), although over shorter distances. This technique is commonly used in applications such as 3D sensing of shapes inside robotic surgical catheters and for high-resolution strain mapping of wind turbines and composite aircraft structures (Ding et al., 2023, p. 26932). BOTDA technique induces Brillouin scattering in the optical fiber by exciting a pump pulse as well as a counter-propagating probe within the fiber. The gain induced in the probe due to the Brillouin frequency shift provides information on temperature and strain along the fiber with an accuracy of around $1℃$ and 20 $\mu\varepsilon$, respectively, with a spatial resolution of *0.1-1m* over tens of kilometers (Wang et al., 2026, p. 231). This technique is used to monitor pipelines, tunnels, and dam bases (Ashry et al., 2022, p. 1421).

3.3.2 Plasmonic and Nanophotonic Platforms

Plasmonic and nanophotonic sensing devices rely on the interaction of light with nanoscale metallic or dielectric components to reach sensitivities and spatial confinements that are inherently impossible using traditional optical systems. Plasmonics deals with the excitation of light into collective electronic oscillations at the boundary of a metal with a dielectric material to produce intense electromagnetic fields, which are highly responsive to variations in the local refractive index (Kazanskiy et al., 2023, p. 2). Surface plasmon resonance (SPR)-based plasmonic sensors represent the most commercially developed nanophotonic sensing system, wherein SPR biosensors quantify real-time interactions between biomolecules immobilized onto an optically active gold film without the use of fluorescent tags, achieving applications in rapid virus detection, allergy tests for food proteins, and clinical diagnosis (Taha, 2021, p. 2). The most rapidly evolving sensor technology is that of Localized Surface Plasmon Resonance (LSPR) based on metallic nanoparticles (usually gold and silver), which obtains highly

sensitive sensing with application in biosensing chips for pathogens detection. The dielectric nanophotonic sensors utilize the optical resonance in high-refractive-index nanostructure such as silicon ring, disc and slot, where resonant mode frequency changes with local refractive index. Silicon microring resonator that has shown multiplexed biosensing capability with an excellent sensitivity in detecting protein biomarker down to attomolar level is one of the main application areas (Inan et al., 2017). On the other hand, the photonic crystal sensors benefit photonic crystal (periodic dielectric structure) that creates a photonic bandgap and resonance spectrum which are shifted by surrounding refractive index. Photonic crystal nanocavity coupled to tapered optical fiber is demonstrated for sensing gases with sensitivity of 0.19 nm per 10^{-3} RIU change in refractive index (Taha, 2021, p. 10). The latest technology within this sub-classification is metamaterial and metasurface sensors. Via altering the geometry of the sub-wavelength unit cells of a metasurface, resonances can be created at any desired wavelength, with confinement to a great extent. As such, these can enable the sensing of molecules at terahertz frequencies, perfect absorber sensors for gas detection, and thin film optics sensors (Khonina et al., 2023, p. 10).

3.3.3 Quantum Optical Sensor Platforms

Quantum optical sensing platforms constitute the cutting edge of sensing devices, taking advantage of non-classical features of light and matter such as entanglement, squeezing, and single-photon statistics in order to obtain precision beyond what is possible by using classical light sources. This occurs because the states of light used in quantum optical sensors allow surpassing the standard quantum limit, which determines the fundamental limitations of any classical optical sensor, and therefore making possible an infinite sensitivity enhancement by means of entangled photon pairs or squeezed vacuum states (Senkans et al., 2026, p. 25). There are two major classes of quantum optical sensors. Quantum enhanced optical readout sensors employ non-classical light – entangled photons, squeezed light, or single photons in interferometers and imaging systems. Entanglement-based sensing systems employ pairs of photons that are injected in both paths of an interferometer, yielding a phase sensitivity scaling with *1/N* rather

than the classical *1/√N* shot-noise limit, also known as Heisenberg-limited sensing. This technique has been implemented in gravitational wave detection experiments and is currently being explored in applications to medical imaging with low dose irradiation (Giovannetti et al., 2004, p. 6). Squeezed-light sensing, which involves quantum noise reduction below the shot noise limit in one quadrature of the light, has also been applied to the Advanced LIGO gravitational wave detector to extend its detection range and enable detection of gravitational waves which their quantum noise is dominant. Single-photon sensing techniques involve the use of avalanche photodiodes and superconducting nanowire single-photon detectors to detect and count individual photons and have applications ranging from quantum key distribution networks to long-distance LiDAR with centimetre-range precision.

Quantum matter sensors involve the quantum mechanical characteristics of selected material systems. Defect centers in solid-state platforms, particularly nitrogen-vacancy (NV) defects in diamond, rely on the quantum mechanical spin state of individual defect atoms for measurements of magnetic fields, electric fields, and temperature with nanometer-scale spatial resolution, therefore making possible microscopic MRI of individual neurons and mapping of magnetic fields generated by single cells through action potentials (Rondin et al., 2014, p. 22). Femto-Tesla detection of magnetic field via atomic resonance sensors employs the fine quantum resonances exhibited by alkali metal atoms such as rubidium and cesium trapped in an optical cell and is currently being applied as wearable devices for detecting brain waves using MEG neuroimaging technology. Rydberg atom detectors rely on the extremely high polarizability of atoms in the high principal quantum state achieved via the process of two-photon excitation. The sensitivity of Rydberg atom detectors to electric fields increases according to the power law n^7 with respect to the principal quantum number. This feature makes the detecting microwave and terahertz fields possible (Senkans et al., 2026, p. 25).

3.3.4 Imaging and Vision-based Systems

The sensor architecture based on imaging and vision technology collects optical information in a distributed form in a two-dimensional observation space, in contrast to a pointwise or linear fashion. This implies that the information contained in the sensor output is fundamentally distinct from the traditional scalar or one-dimensional output of the measurement variable. The sensors in this sub-classification are categorized according to their respective imaging modes into three categories.

The most frequently utilized method in this group is the intensity imaging system. In this system, a two-dimensional detector array senses the spatial distribution of optical energy. Intensity imaging involves the use of hardware such as charge-coupled device (CCD) or complementary metal-oxide semiconductors (CMOS) cameras. In an array of CCD or CMOS, each individual pixel detects the intensity value at a certain point and together they form a complete two-dimensional image. This technique serves as the basis for machine vision techniques utilized in manufacturing processes, surgical procedures, and autonomous vehicles, among others.

Spectral imaging represents a more advanced form of intensity imaging which uses a spectrum of wavelengths instead of an individual broadband wavelength for taking an image. The spectral data gathered with the aid of the sensor allows the system to determine what materials exist in the scene, apart from their location in space. Multispectral imaging systems capture images using 4 to 15 bands of spectrum, while having multiple applications in the agricultural sector such as sensing plant stress, detecting pests and yield prediction when mounted on drones. Hyperspectral imaging systems go a step ahead of multispectral imaging systems, where they take hundreds of narrow bands of spectrum continuously, forming a complete fingerprint of each pixel in the image. Some of its major applications include satellite-based mineral mapping, food safety inspection in conveyors and surgical tumor margin detection (Gorji et al., 2024, p. 8).

Computational and advanced imaging technologies involve multiple architectures that are more than just capturing intensity or spectral information but rather require computational processing to create an image that would be impossible to generate via normal optics. Point, line, and area scanners employ mechanical or optical scanning of the scene to create an image pixel-by-pixel and provide the backbone of confocal microscopy and hyperspectral push-broom imagers used by satellites. In the concept of ghost imaging, the object's image is generated using photons that do not even touch the object being imaged but correlate spatially with a reference beam according to classical or quantum mechanics and has uses for imaging objects through scatterers. One particular field of computational imaging that has seen rapid growth and significance is super-resolution microscopy, which beats the classical diffraction barrier of light, typically around 200 nanometers laterally, that sets the limits of resolution for ordinary optical microscopes. There are four primary forms of super-resolution microscopy, each utilizing a different physics mechanism.

Stochastic Optical Reconstruction Microscopy (STORM) technique was developed by Rust, Bates, and Zhuang in 2006 (Rust et al., 2006). STORM relies on the property of some fluorescent probes that allow them to be alternated from an emitting state to a non-emitting state depending on the intensity of light exposure. STORM captures super-resolution images based on the localization of randomly activated fluorescent markers by acquiring thousands of localization positions for individual molecules sequentially imaged during each frame. STORM has a lateral resolution of 20 nm (Rust et al., 2006, p. 793) and has been used for imaging the organization of actin fibers, clathrin-coated pits, and membrane proteins in living cells.

Photoactivated Localization Microscopy (PALM) technique relies on the same single molecule localization principle employed by the STORM method, except that instead of using photo switching dyes, PALM exploits photoactivatable or photoconvertible fluorescent proteins, such as PA-GFP and mEos. This involves turning on a small number of molecules with short pulses of UV light, imaging them until bleaching, before

activating another small group of molecules, repeating the process thousands of times. The reconstruction of the localized coordinates of the molecules gives rise to an overall super resolution image. Since the fluorescent proteins used in PALM are genetically encoded, it makes it ideal for performing live cell experiments on particular proteins in cells. Indeed, PALM has been used to determine the arrangement of certain focal adhesion proteins and plasma membrane organization at 30nm resolution (Betzig et al., 2006, p. 1645).

Stimulated Emission Depletion (STED) Microscopy relies on an entirely different way of breaking the diffraction limit by confining the effective fluorescence emission volume to being smaller than the diffraction limit via a physical method. Specifically, a STED microscope uses a conventional focusing excitation laser beam together with a laser beam of doughnut shape which stimulates emission of the fluorophore from the excited to the ground state without a corresponding photon emission (Hell & Wichmann, 1994). STED microscopy provides images with a resolution of about 30-80 nm for biological samples and less than 10 nm under specially optimized conditions. As opposed to localization techniques, STED is a scanning technology capable of obtaining images faster, thus making it more suitable for live cell imaging applications, such as synaptic vesicle recycling and mitochondrial fission (Klar et al., 2000).

Structured Illumination Microscopy (SIM), a relatively new technique that employs patterned illumination of the specimen rather than uniform illumination to achieve super-resolution, follows a completely different approach. In SIM, the specimen is illuminated with sinusoidal striped patterns of light at various orientations and phases. The interference between the patterned illumination and the fine structure of the specimen causes the generation of Moiré fringes that encode the high-spatial frequencies of the specimen structure, which would otherwise be beyond the resolving power of the microscope (Gustafsson, 2000, p. 82). Therefore, by decoding the encoded high-spatial frequencies from the generated Moiré fringes in several orientations, an image with super-resolution is obtained with lateral resolution ranging between 100 and

120 nanometers, which is twice as good as the resolution offered by a conventional microscope. Although SIM does not provide the same amount of resolution enhancement as STORM, PALM, and STED, it requires only low laser intensities, can use any fluorophores, including fluorescent proteins, and allows for imaging live specimens at very high frame rates (Gustafsson, 2000).

3.3.5 Remote Optical Sensing

Remote optical sensor systems take readings at a distance, usually from airplanes, satellites, or ground stations, without direct contact with the object being studied. These sensors can be categorised as passive or active sensors based on the nature of their energy source. Passive remote sensors utilise either the sunlight that is reflected off the Earth's surface or the thermal energy emitted by both the surface and atmosphere for analysis purposes. Multispectral or hyperspectral remote sensing using passive sensors from satellites and aircrafts serves as the basis for mapping vegetation conditions, lake and coastal water quality assessment, soil moisture content analysis, and land-use studies. Landsat, Sentinel-2, and AVIRIS are examples of such instruments and most popular remote sensing platforms. Reflected imaging is dependent on the unique spectral and angular features of the solar radiation that has been reflected off the surface. Infrared thermography relies on the thermal radiation emitted by objects within the 8–14 μm atmospheric window transmission region to generate maps of thermal distribution in a non-contact manner. The application areas include energy audits of buildings, electricity grid fault analysis, industrial processes, and drought-induced stress in agriculture, and it is one of the rapidly growing types of remote sensing technology due to the availability of low-cost uncooled microbolometer detector arrays (Meng et al., 2026b, p. 159). In active remote sensing, the object being measured is illuminated with its own light source, while the reflected light or the backscattered light is detected by the instrument. Range-finding and mapping systems, including LiDAR (Light Detection and Ranging), illuminate the scene using pulsed or frequency-modulated lasers to determine the time of flight of the photons returning to construct a three-dimensional point cloud of the scene. LiDAR has become an essential component on self-driving cars,

estimating forest biomass, building structures, and discovering ancient ruins, and Geiger-mode LiDAR on satellites is beginning to provide global canopy height maps.

Atmospheric spectroscopic active remote sensing employs tunable lasers to measure the differential absorption of specific gases in the atmosphere by the laser beam. This is the DIAL (Differential Absorption LiDAR) method that has been proven successful in performing accurate measurements of the atmospheric column density of carbon dioxide, methane, ozone, and water vapor in addition to passive measurements of greenhouse gas satellite monitoring systems (Wagner & Plusquellic, 2016, p. 6293). The Laser Induced Breakdown Spectroscopy (LIBS) and Laser Induced Plasma Spectroscopy involve the application of a high-power laser pulse to produce a micro-plasma on the surface, which allows the analysis of the ablated material through its atomic emission spectrum. It is becoming more common in planetary surface investigation, heritage evaluation, and material sorting (David A. Cremers, 2013, p. 28).

3.4 Category IV: Application Domains

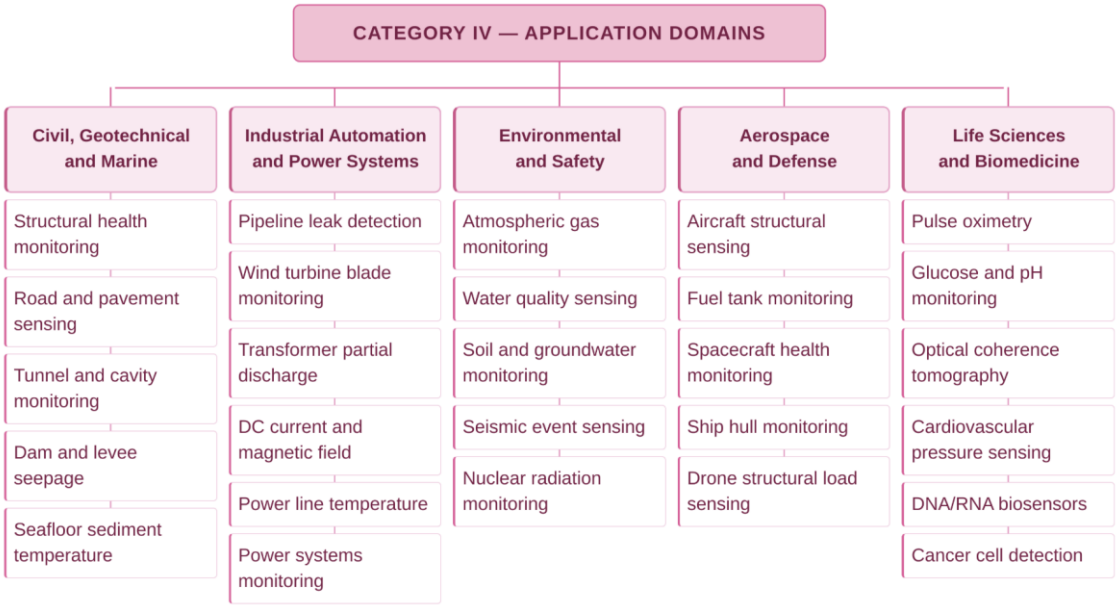

Figure 8. Category IV: Application Domains

Figure 8 shows the applications of optical sensing technology in different industries ranging from Geotechnical to power systems and from environmental aspects to life science domain. Measuring DC current and magnetic fields is one of the most technically demanding and commercially significant subcategories in modern electrical engineering, power systems, and physical metrology. The following review summarizes recent scientific literature contributions in peer-reviewed journals, while focusing on fiber-optic sensing technologies that have been studied, developed, and applied for DC currents and magnetic field measurements. The review is organized according to applications area, which includes, in order, the metal electrowinning and electrolytic processing industry, high-voltage direct current (HVDC) power transmission, smart grid and power quality monitoring, geomagnetically induced current (GIC) detection in power transformers, nuclear fusion plasma diagnostics, electric vehicle battery management, and biomedical magnetometry.

Metal Electrowinning and Industrial Electrolysis: Fiber optic current sensors using the Faraday effect principle have been developed and used for measuring currents on the DC bus in aluminum, copper, and zinc smelters up to 500 kA (Bohnert et al., 2005, 2007). The sensors are placed around existing bus bars in an epoxy-coated flexible strip without any need to disturb the electrolysis process and have an accuracy within ±0.1% (Bohnert et al., 2007, p. 3602). They have significantly improved performance compared with Hall-type sensors that can drift at these currents (Bohnert et al., 2005).

High-Voltage Direct Current Transmission: Fully fiber optic Sagnac interferometry FOCS systems have been installed in HVDC stations up to *±800 kV* in operation, conforming to metering accuracy class 0.2 in compliance with *IEC 60044-8* standard for revenue grade direct current measurements (Liu et al., 2022, p. 604). The sensors have no saturation due to DC and also ensure complete galvanic isolation from the high voltage conductor. The new deployment in the windings of a power transformer ensures that a single fiber can measure both current and temperature (Wu et al., 2022, p. 1).

Smart Grid Monitoring and Power Quality: Nano-ferrofluid multimode interferometric fiber optic sensors have shown simultaneous sensing capabilities of both direct and alternating currents up to 15 kHz, thus facilitating detection of current faults in output stages of power electronic converters beyond the scope of existing current transformers (Karki et al., 2024, p. 26894). This directly solves the challenge of measuring the increasing DC component and harmonics being produced from inverters of renewable energy sources into the grid. On a larger scale, a general review of nanodielectric materials for optical sensing can be mapped to smart grid applications such as transmission line sensing and circuit breaker evaluation, and distributed energy resource management within IoT energy internet platforms (Zhang et al., 2023, p. 116).

Geomagnetically Induced Current Detection: A low-cost single-mode fiber FOCS placed on 380kV transformer phase conductor was able to detect biases of 1 Amp DC, resulting from a G3 class solar event in January 2025, indicating for the first time ever, geomagnetically induced current exists within non-earthed transformer high voltage phases (Mandl et al., 2026, p. 4) .The FOCS also helped to identify the complete AC signal together with even harmonics along with the DC bias signal, making it possible to determine core saturation probability (Mandl et al., 2026, p. 6).

Nuclear Fusion Plasma Current Measurement: The effectiveness of fiber optic current sensors as the chosen method for measuring plasma currents in ITER has been verified, where there is a need to monitor DC plasma currents of several mega-amperes in a high neutron flux environment (Dandu et al., 2023, p. 1). Polarization-based distributed reflectometry, which was developed in the JET machine, gives the field profile in the poloidal direction instead of the total plasma current and as a result reconstructs the distribution of plasma currents (Dandu et al., 2023, p. 8). Testing in the D-T fusion phase of JET showed that the FOCS technology can meet the ITER demands despite 14 MeV neutron exposure (Gusarov et al., 2025, p. 1).

Electric Vehicles and Battery Management: Fiber-optic sensors have been recognized as one of the best sensing technologies for measuring branch currents in the narrow confines of lithium-ion battery pack interconnects in electric vehicles, in which conventional Hall effect sensors face problems of mutual magnetic interference between parallel cell interconnects as well as inadequate spatial selectivity in discriminating the different branches(Su et al., 2021, p. 11). Precise sensing of branch currents is required to estimate states of charge and health in battery management systems of electric vehicles and power grids. However, the main obstacle to implementation lies in the cost of optical interrogators rather than in the performance of sensors themselves (Su et al., 2021, p. 25).

Biomedical Magnetometry: Room temperature single-beam all-optical magnetometers that work at Earth's ambient DC field strength have been experimentally implemented for non-zero field magnetocardiography and magnetoencephalography without a magnetic shielded room (Petrenko & Vershovskii, 2022, p. 1). The intrinsic all-optical gradiometer using non-linear magneto-optical rotation provided a noise level down to 18 *fT/cm/VHz* with a common mode rejection ratio up to 30 *dB* at Earth's ambient DC field and is suitable for medical applications in clinical magnetocardiography (Cook et al., 2024, p. 1). Also, a quantum enhanced optical current transducer with nitrogen-vacancy centres in diamond and single fiber coupling has been suggested for DC current monitoring in smart grids with a sensitivity in the picotesla regime (Dang et al., 2026, p. 197). Table 2 summarizes all the applications of fiber optical sensing technologies in the measurement of DC current and magnetic field.

Table 2. Applications of Fiber Optic Sensing for DC Current and Magnetic Field Measurement

SECTOR	SENSOR TECHNOLOGY	PHYSICAL PRINCIPLE	DC RANGE / ACCURACY	KEY ADVANTAGES	KEY LIMITATIONS
Metal electrowinning electrolysis	flexible epoxy-strip coil wound around bus bar	Faraday magneto-optic effect, polarisation	DC up to 500 kA; accuracy ±0.1%	No magnetic saturation; EMI immune	Verdet constant varies with temperature;
High-voltage direct current	Sagnac interferometric; inside transformer windings	Faraday magneto-optic effect;	DC up to ±800 kV; 0.2 metering accuracy	No DC saturation; full galvanic isolation;	High unit cost; spun PM fiber required;
Smart grid and power quality	Nano-ferrofluid and nanodielectric optical sensors	Magnetic-fluid refractive index modulation	DC field baseline + AC up to 15 kHz	Simultaneous DC + harmonic sensing; low-cost fabrication; IoT-platform compatible	Ferrofluid ageing and temperature cross-sensitivity
Geomagnetically induced current detection	Single-mode fiber with adjustable phase retarder on 380 kV phase conductor	Faraday magneto-optic effect	DC bias down to 1 A	Low-cost design; installed on energised conductor without service interruption	Sensitivity limited at low DC by AC interference
Nuclear fusion plasma current measurement	Reflective FOCS and sensor on tokamak vacuum vessel	Faraday magneto-optic; distributed polarization OTDR	DC plasma current up to 3.5 MA	No drift under steady-state DC	Radiation-induced Verdet constant change requires correction;
Electric vehicles and battery management	Fiber optic sensors	EMI-immune optical sensing;	cell-level resolution	Immune to EMI; explosion-proof in electrolyte environment	High optical interrogation system cost
Biomedical magnetometry	NV-centre diamond quantum current transducer	Non-linear magneto-optical rotation; ODMR spin-state readout	MCG ~100 pT; MEG ~10–100 fT; NV picotesla DC sensitivity	Room-temperature; no cryogenics; wearable clinical deployment	DC drift under patient movement; laser frequency stabilisation required;

4 Case study: Suvilahti Seabed Sediment as a Renewable Urban Heat Source

With the increasing need for decarbonization of urban heat production, there has been a resurgence in interest regarding shallow geothermal systems that do not require deep drilling techniques. The seabed sediment, which occurs at the interface of aquatic and terrestrial urban environments, presents another potential geothermal source. In contrast to traditional bedrock boreholes, inadequate heat extraction by the bedrock borehole will occur when the size of the borehole is not properly sized (Andersson & Gehlin, 2018). However, the seawater that overlays the sediments acts as a conduit for solar recharging annually. This raises the question of whether solar recharging of the sediment layer is enough to maintain sustainable extraction during harsh northern European climatic conditions. This chapter presents a case study of the Suvilahti sediment heat system, located about three kilometers to the south of Vaasa city center, along the western coastline of Finland (latitude ~63°N).

The Suvilahti project, which was launched around the time of the 2008 Vaasa Housing Fair, was the first implementation of seabed sediment heat as the main source of heating energy for a whole residential area in Finland (Hiltunen et al., 2017). During the next ten years, it developed into a distinct outdoor research facility generating a multi-year data set for the present analysis. Heat is extracted from the seabed sediment through a network of horizontal directional drilling (HDD) pipes laid three to four meters deep into the sediment layer starting from the top of the seabed surface (Mäkiranta, 2020, p. 8). The total length of pipes laid is 7,800 meters split into two separate pipe systems, which start from Liito-oravankatu and Ketunkatu. Each of the two separate pipe systems includes a heat collecting pipe of 300 meters and an accompanying optical fiber sensor of 300 meters each. The novel design of the pipe called a "flower cross section pipe," later branded as Refla, was invented to increase the surface contact area between the heat carrier and sediment (Hiltunen et al., 2017, p. 400).

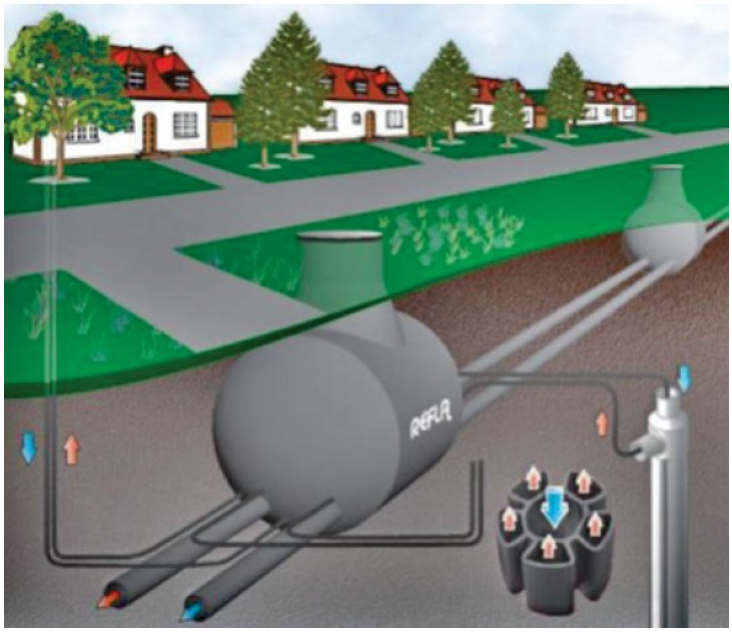

Figure 9. Cross-sectional schematic of the Suvilahti sediment heat-collection system (Hiltunen et al., 2017, p. 51)

Figure 9 shows the diagram of Suvilahti sea sediment heat collection system with the underground piping network, REFLA distribution well, and heat collection piping with the cross-sectional structure of "flower." The blue arrows show the heat carrier fluid flowing out from the REFLA system towards the sediment field, while the red arrows depict its return flow after heating back to the REFLA distribution well and residential housing structures. This novel design of the pipe shape ensures maximum thermal exchange with the sediment layer, resulting in heat collection efficiency of 40-50 W/m.

4.3 Research Methodology

The empirical basis for the current case study is provided by a experimental research program carried out using two specialized open-air testing grounds located in the Suvilahti region. The primary measurement method used in the Suvilahti study was Distributed Temperature Sensing (DTS), using Raman backscattering algorithm. A DTS measurement system uses short pulses of a laser sent through a glass-fiber cable; part of the energy is backscattered at each point in the fiber, and temperature can be continuously reconstructed from the intensity of the temperature-dependent Anti-

Stokes Raman band along the entire length of the fiber. To achieve the highest quality measurements and to enable differential calibration, the double-ended measurement approach was used, where both ends of the cable were connected to the measuring equipment (Van de Giesen et al., 2012, p. 5471). The measurements were done using a Sensornet Oryx DTS devise that offers temperature accuracy of ±0.5°C and a spatial resolution of 1 meter. The duration of each measurement run was ten minutes, during which twenty individual readings were taken for each channel; the sediments' temperature at a specific point is the mean temperature of eight readings taken during the same run. Calibration was conducted against the Pt100 resistance temperature detector (accuracy ±0.25°C) at the beginning of each field run by using a patch cable that goes through an ice-bath to give the reference temperature (Mäkiranta, 2020, p. 16).

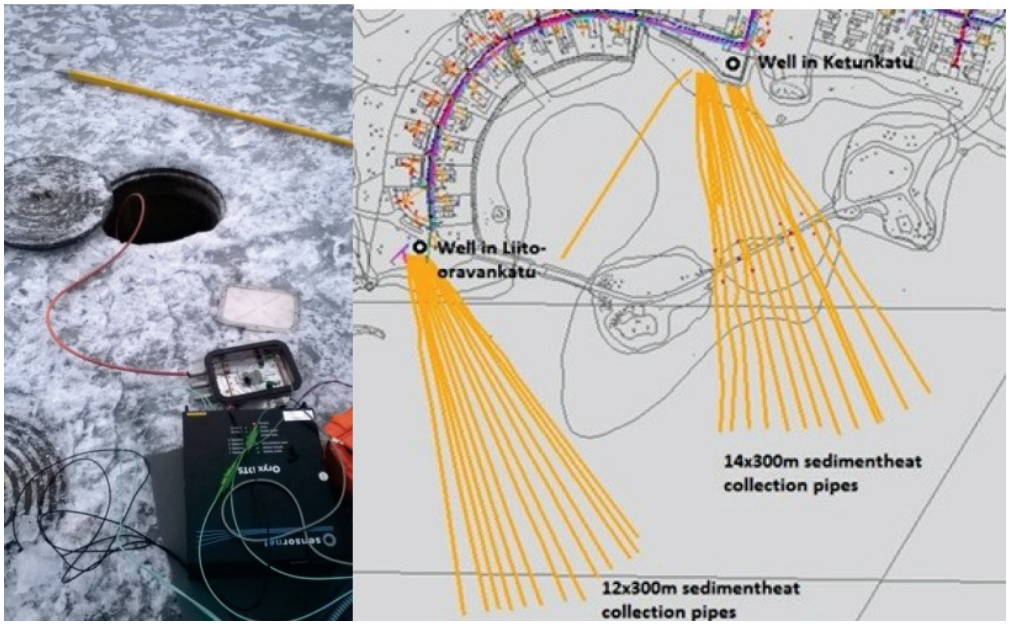

Figure 10. Left: Sensornet Oryx DTS device. Right: Spatial layout of the two sediment heat-collection branches (Mäkiranta, 2020, p. 12).

Figure 10 illustrates the Sensornet Oryx DTS measurement instrument installed using an ice-drilled borehole at the Suvilahti research site during winter season operation. The system is used to measure Raman backscattering signals along the optical fiber, which enables the continuous measurement of sediment temperatures in 1-meter intervals over the entire 300-meter length of the cable. Plan view map of the Suvilahti coastal area

is also depicted in figure 10, showing two heat collection branches, consisting of 12×300-meter pipes connected to the well located in Liito-oravankatu and 14×300-meter pipes connected to the well in Ketunkatu, both with optical fiber DTS cable.

The major source of uncertainty for the temperatures in the Suvilahti data comes from the placement of the optical cable on the outside surface of the heat carrier fluid pipe instead of being embedded directly into the bare sediments. In theory, the heat carrier fluid that flows inside the pipe can affect the temperature of the immediate surrounding sediments and hence cause an error in the DTS measurements. Nevertheless, according to (Mäkiranta, 2020), the effect is unlikely to be significant because of the mass of the sediments and the slow flow of fluids due to low enthalpy extraction. The accuracy of the data can be further confirmed by the consistency of the temperature data obtained for the two branches under similar seasonal conditions.

4.4 Results analysis

Figure 11 illustrates the average temperature for March sediments based on the distance from shore on the Ketunkatu branch from 2014 to 2016. In the near-shore area (up to 0-20 metres), the temperatures were at their minimum levels and approached zero degrees Celsius, especially in March 2016 when the temperature was about -1 °C. The low temperature zone close to shore is a result of the immediate impact of winter cold, shallow depths, and proximity to the air-sediment interface, since the latter responds directly to changes in atmospheric conditions. After around 20–25 metres from the shoreline, the consistent increase in temperature occurs, resulting in a rapid temperature increase to 4–5 °C. This is due to the fact that the thickness of the overlaying water layer is sufficient enough to prevent any cooling of the sediment through the insulating property. After this sudden increase in temperature, there is a relatively constant period ranging between 25 and 100 metres, when the temperature stays almost steady. This is an indication of the equilibrium between heat removal and thermal balance.

After about 120 metres, a sustained increase in temperature can be noticed in all three profiles, which ends up in 6.5–7.1 °C by the time it reaches 295 metres from the shoreline (the distal part of the pipe).

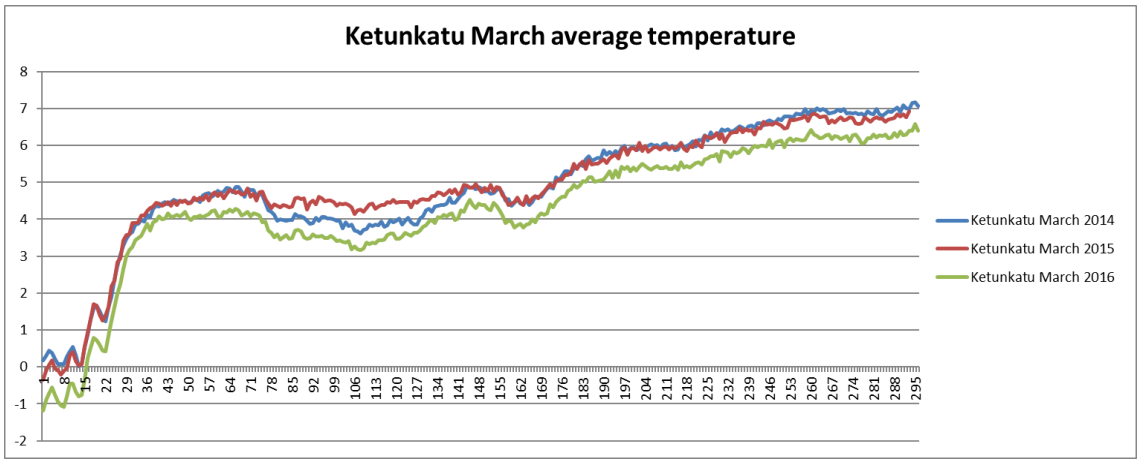

Figure 11. Average March sediment temperatures (°C) along the Ketunkatu

The green line representing the 2016 profile is slightly below both other lines near the shoreline yet starts approaching them further away from the shore starting from around 150 meters. Such an approach to each other with increasing depth shows that the thermal regime of the sediments deep down into the ground is quite stable over the years despite inter-annual variability in winter air temperatures on the surface.

Figure 12 illustrates the complete annual sediment temperature cycle using the DTS method recorded along the Ketunkatu branch in 2016 where sediment temperatures were compared to distance from shore along the entire 295-meter-long cable. The figure can be divided into four distinct thermal zones that have distinct thermal behavior patterns and seasons and provide information on the thermal regime regulating the sediment heat storage at the Suvilahti site.

Zone I: Near shore Zone (0 – 25 m).

The most thermally heterogeneous area is that of the near-shore zone, which experiences the greatest variation in seasonally changing temperatures in this water

body, and all vertical profiles indicate significant changes in temperatures. In July, near-shore temperatures achieve their peak in approximately 17-18°C at the length of up to five metres, after which they fall off rapidly. This is the maximal thermal range in the water column of the entire set of observations, caused by its relatively shallow depth and direct influence of solar radiation on its sediment bottom. A similar pattern was observed for June, with near-shore temperatures peaking around 13-14°C.

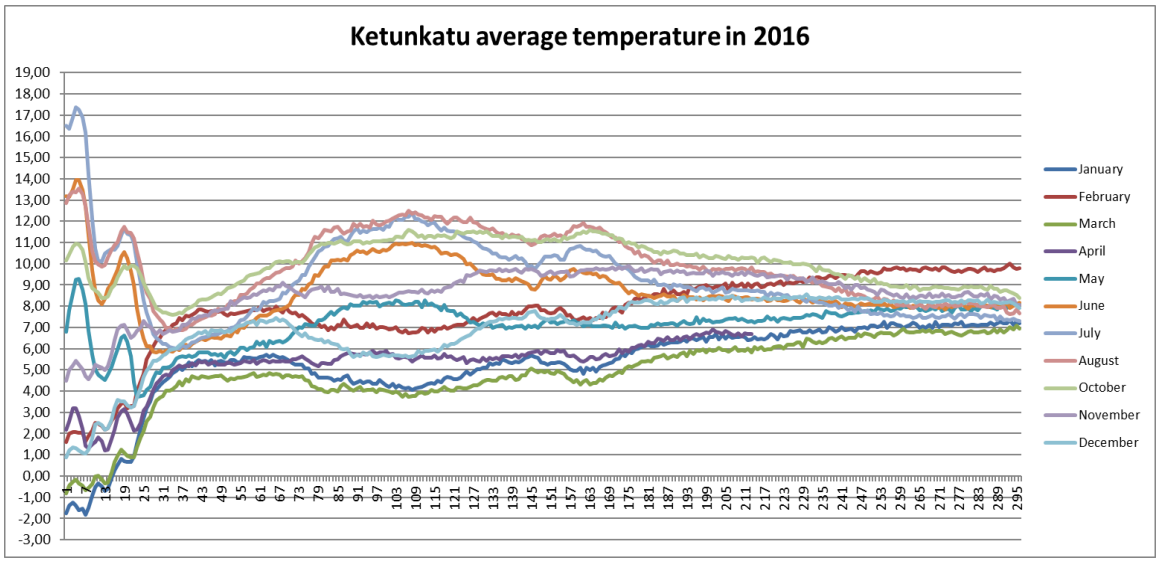

Figure 12. Monthly average sediment temperatures (°C) along the Ketunkatu branch in 2016

In contrast, two winter months, January and February, show that they are characterized by low near-shore temperatures of about -1.5 °C close to shore. The high summer peaks, with zero or sub-zero winter temperature, in this area create an annual amplitude difference of about 19-20 °C for the first 25 metres, which is the highest among all profiles. The near-shore area is thus very unstable and not fit for use in heat collection, explaining why the heat-collecting pipes should be located 3-4 metres into the sediment layer.

Zone II: Transition Zone (25 to 60 meters).

There is a sharp convergence of the monthly measured temperatures around 25 meters away from the shoreline. The extreme values recorded in the nearshore area converge

quickly into a tight range of temperatures, where most of the months fall between about 4 to 8 °C at 60 meters. This occurs due to the fact that the sediments resist the effects of temperature variations with an increase in thickness and distance from the shoreline. This is because such characteristics act as a buffer for the temperature variations in the atmosphere and surface water. This zone represents a crucial thermal boundary since beyond this point, the sediment behaves as a stable and exploitable heat reservoir instead of a volatile surface layer.

Zone III: Middle Zone (60 – 170 meters).

Seasonal patterns reemerge, although in a more organized manner, in the middle layer, where summer and autumn seasons, particularly those of August and July, include the upper portion of the temperature profile with maximum temperatures of approximately 11-12°C at the length of 100-130 meters. Conversely, winter months ensure the lower temperatures of around 5-7°C. Winter months, meanwhile, maintain the lowest temperatures in this range (about 5-7°C). The months of March, April, and May are placed in the middle category, with temperatures gradually rising throughout the year. An important observation in this section is the relative location of the curves during the fall months. Temperatures in October and November are comparable to or even above summer temperatures while the climate was relatively cold at that period of time. This discrepancy can be explained by the one to two-month lag between the atmospheric influence and temperature changes observed within the sediment, reported by (Hiltunen et al., 2017). In other words, sediments keep releasing stored summer heat for a while, which means that October-November would be the thermally richest period of the year for heat recovery purposes.

Zone VI: Distal Zone (170-295 meters).

Beyond the distances of 170-200 meters from shore, the progressive convergence continues this time towards an end-point stable temperature range of 7-10 °C at 295 meters away from shore. The month of August holds the highest distal temperature of approximately 10 °C, while January and February are stabilized at the lowest possible

range of about 7 °C. Therefore, the total amplitude of the distal season range reaches around 3-4 °C only, which is extremely reduced compared to the 19-20 °C found at closer shores. This distal convergence is highly important for two reasons. Firstly, this indicates the reduction in influence of atmospheric seasonality due to increasing distance; hence, proving once again the existence of the natural thermal flywheel that can absorb energy during longer periods. Secondly, the presence of positive temperatures at all points of the annual cycle and throughout all months (7 °C and above) shows the fact that the thermal reservoir of the sediment layer is not depleted at this distance and any month within one year.

In conclusion, the thermal contrast in the near-shore areas must be excluded from heat extraction. The mid zone, being characterized by pronounced seasonality, when autumnal temperatures peak, is the most effective for energy production. The distal zone, although it is thermally stable, gives less temperature peaks which makes it less important for system operation of heat consumption. Effective management of heat extraction distribution along the pipes will increase the productivity of energy production and sustainability of the system operation if it is applied more efficiently in the 60-170 m zone.

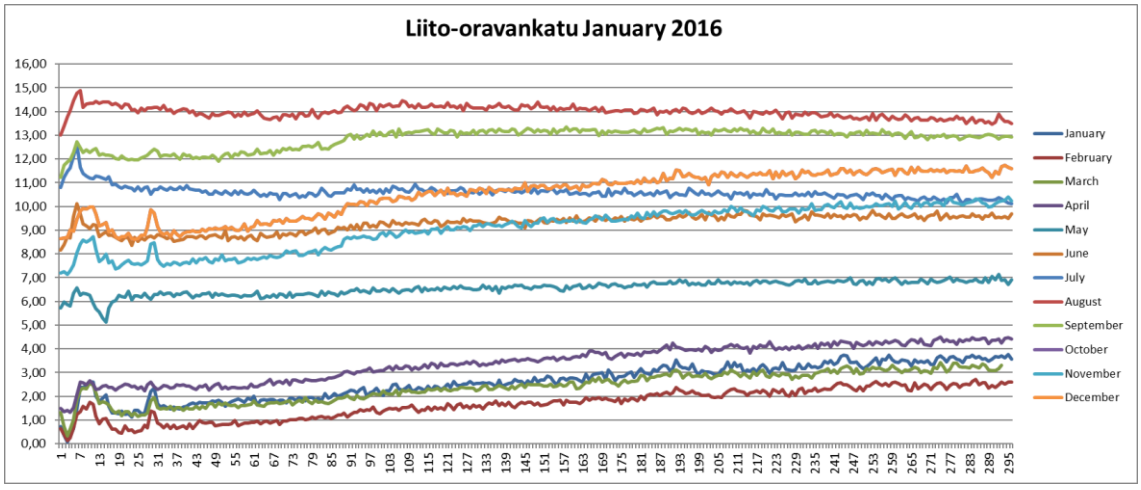

Figure 13. Monthly average sediment temperatures (°C) along the Liito-oravankatu branch in 2016

Monthly measurement of sediment temperatures in the Liito-oravankatu branch during 2016 are displayed in Figure 13. Several months reveal small oscillations and irregularities in the vicinity of the shoreline, specifically in June and November due to higher sensitivity of shallow sediments to thermal changes occurring on the surface. However, starting from around 25 m, sediment temperature in all months become steady and follow a continuous trend for the whole span of the cable. Against the convergence toward the distal end in Ketunkatu, a seasonal and well separated stratification is maintained across the entire 295-metre. The temperature in August obtains the highest amount of about 14-15 °C and those of February and September are the lowest at 1-3 °C. The trend indicates the typical temperature lag effect for the sediments, with the heat stored from the previous autumn season still remaining unremoved during the month of February, whereas the heat from the sediments in the late summer had been partially removed in the previous winter removal process. During the winter season, the temperatures measured in January and October remain comparatively low yet above zero at around 3-4 °C, demonstrating the fact that no freezing point is reached even by the coldest period of the year. In general, the stable separation of monthly trends in the entire length of the cable proposes the uniform behavior of the heat flow in the Liito-oravankatu branch, making it sustainable and predictable.

4.5 Proposed algorithms for future analysis

Given that there is noise in the signals, invalid temperature readings, calibration inaccuracies, and varying heat conductivity, a preprocessing procedure to remove the anomalies within the raw data collected using the DTS system, would be beneficial. For instance, algorithms such as Isolation Forest or autoencoder-based deep learning networks could be used to detect statistically questionable readings due to sensor deterioration, cable tensions, and ice barriers preventing physical access to the wells located at Liito-oravankatu and Ketunkatu. Other than anomaly detection, some Machine Learning algorithms can developed to model the relation between the Stokes,

Anti-Stokes Raman scattering signal, fiber distance, temperature slope calibration, k internal, k external, internal reference temperature, external reference temperature, and temperature readings, allowing for a more consistent spatial temperature profile despite the high thermal gradients near the shoreline.

In addition, some unsupervised clustering algorithms like k-means clustering can be employed to automatically differentiate different sediment zones and detect transitions in thermal behavior along the full 295-metre cable length. This objective means of classifying zones eliminates the element of subjectivity involved in identifying the zones by visual inspection and will give clear spatial boundaries between the near-shore unstable zone, the buffer zone, and the distal stable zone, aiding in future pipe placement for sediment heat systems. Models of supervised learning, for example, Random Forest regression model and Gradient Boosting algorithm, may then be applied to learn from the preprocessed historical data set of DTS and forecast future monthly profiles of sediment temperatures using independent variables like air temperature, inlet and outlet temperatures of the heat carrier fluid, and seasonality indicators. Considering the well-known correlation between atmospheric forcing and sediment temperature response demonstrated by Mäkiranta et al. (2020), it is likely that such models will provide accurate spatial temperature forecasts in the short term for the entire profile.

5 Conclusion and future works

5.1 conclusion

The present thesis focuses on addressing two closely related issues in the field of optical sensing technologies. First, it aims to develop a comprehensive multi-dimensional classification system capable of providing a structured overview of the wide range of advanced optical sensing technologies. Second, it provides a practical verification of one of the proposed techniques through a case study. Both objectives have been addressed through a systematic literature review, taxonomy development, and a field experiment conducted at the Suvilahti seabed sediment heat system in Vaasa, Finland.

From the systematic literature review on the existing classification systems, it appears that while some classifications may be provided by individual studies, these tend to be incomplete and specific only to a certain domain. Most previous work on classification uses just one parameter to classify sensors, namely scattering type (Rayleigh, Brillouin, Raman), sensing method (FBG, tapered, PCF), or the application area. There is, however, no classification which includes all the parameters that characterize the optical sensors, from their signal physics perspective to their architectural considerations. This gap motivated the construction of the taxonomy presented in Chapter 3. The proposed taxonomy is based on six criteria which together describe the operation of the sensor, its physical architecture, the measured physical or chemical quantity and its location. They include: (1) light-matter interaction mechanism; (2) sensing configuration; (3) signal detection method; (4) spatial sensing method; (5) target phenomenon; and (6) operational spectrum.

This taxonomy systemically categorizes optical sensing technologies into four groups. The first category divides sensors according to the method of information encoding, which may include modulation of intensity, spectrum, phase, or polarization. The second category considers the fundamental physical mechanism of light-matter interaction in such sensors, which includes absorption, emission, scattering, or nonlinear optics. The

third category differentiates sensors based on their physical implementation, which includes fiber optics, plasmonics and nanophotonics, quantum optics, imaging/vision, and remote sensing. Finally, the fourth category maps optical sensing technologies to the areas of application in which they can be employed, which include power systems, environmental monitoring, biomedicine, and nuclear fusion. It shows how interdisciplinary the majority of optical sensing technologies are and how DC current and magnetic field measurement is the most relevant area for the future directions of this research.

Secondly, the empirical case study carried out in Chapter 4 makes another contribution to the thesis by illustrating the applicability of Raman-backscatter DTS for seabed sediment temperature monitoring at the Suvilahti urban geothermal site. The temperature measurement was done using a Sensornet Oryx DTS system, which was working based on the double-ended calibration method using an ice bath as the reference to yield a temperature accuracy of ±0.5 °C and a spatial resolution of 1 meter along a 295-meter-long optical fiber cable. Different thermal zones were determined based on the analysis of the DTS data obtained during the whole year cycle in Ketunkatu branch. Zone I is the near-shore area starting from 0 to 25 meters. This zone has an extremely changeable temperature throughout the year. The amplitude of the annual temperature change is about 19–20 °C, which means that this zone is not suitable for heat recovery due to its lack of thermal stability. Zone II is the transitional zone from 25 to 60 meters. This zone can be considered as the thermal buffer zone when the extreme values of the near-shore zone rapidly become thermally stable zone of 4–8 °C due to the increasing sediment thickness. Zone III is the middle zone located between 60 and 170 meters. The temperature in this zone has an obvious seasonal change. Summer and autumn months have a temperature of 11–12 °C, while winter months have the temperature of 5–7 °C. Due to the one-two month delay of atmosphere and sediments thermal regimes, October and November are the most suitable months for heat recovery. Zone IV is the distal zone located further than 170 meters, which is stabilized at 7–10 °C with an annual amplitude of 3–4 °C.

These findings clearly indicate that the DTS technology, which employs the Raman backscatter concept and belongs to the scattering mechanism subclass of Category II and the distributed fiber-optic architecture subclass of Category III in the proposed taxonomic scheme, not only has the technical ability to discriminate fine spatial and temporal temperature gradients in the difficult outdoor marine environment but also provides insights for the effective management of sediment heat systems. The case study also directly demonstrates the applicability of the taxonomic approach in terms of how classifying a sensor technology based on its interaction mechanism and architecture directly influences its suitability and performance in practice.

5.2 Future work

The first possible way for future research could be the further expand of the multi-dimensional taxonomy. Although the present taxonomy was based on a qualitative analysis of scientific literature and was developed within this context, it would be interesting for future research to create a more quantitative basis for evaluating different sensing technologies. Such an evaluation can be achieved by introducing certain performance metrics for each sensor that will allow to evaluate such characteristics as spatial resolution, sensing range, accuracy of measurement, sensitivity, technology readiness level, and cost-efficiency. This approach would enable us to make our taxonomy not just descriptive but also a valuable decision-making tool.

Another important approach for future work, would be the use of fiber optic sensors in detecting electric current and magnetic fields. As mentioned in Chapter 3, this is one of the most commercially and technically significant application areas according to the proposed taxonomy. Many conventional sensors have difficulty measuring DC and its corresponding magnetic field. Hall-effect sensors are susceptible to magnetic saturation and thermal drifts at higher currents, Rogowski coils only work for AC measurement, and the core saturation phenomenon prevents current transformers from accurately measuring DC currents. On the other hand, fiber optic current sensors (FOCS), operating

via the Faraday effect, have several advantages over their counterparts. This is because of the polarization angle of light rotation inside the fiber is proportional to the magnitude of the magnetic field. Therefore, FOCS can measure DC currents with linearity from very small currents to even megaamperes. Besides, they give full galvanic isolation, high immunity to electromagnetic interference, and enhanced safety performance, among others. The review of literature performed within this thesis shows the growing relevance of such technology for the contemporary environment.

Following this trend, one of the directions for further research can be an exploration of optical current sensing within the context of a modern data center environment. An FOCS system utilizing the Faraday Effect and Sagnac Interferometer architecture is directly addressing those issues. The main aim of the research project will be to design, calibrate and test the FOCS system by placing it on the DC power distribution busbars of a working data center site, in order to demonstrate the validity of its performance characteristics, such as accuracy, dynamic range and stability, in data center settings. Measurement results will provide the data necessary for characterizing the DC current patterns at the data center facilities, estimating the share of the total consumption provided by each specific load, and checking out the applicability of the FOCS system for incorporating it in a real-time power management platform. The research will also focus on the possibility of using DC current sensing together with distributed temperature monitoring of the same fiber, based on the dual-modulation technique developed recently in the scientific literature for measuring temperatures in transformer windings, leading to an all-fiber optical measurement system for monitoring of power infrastructure in data centers. The expected results from the research will be the development of a validated measurement technique and design guidelines for implementation of fiber-optic current sensors in DC power transmission networks.

Declaration on the Use of Artificial Intelligence

In the preparation of this thesis, an artificial intelligence tool was applied for two specific purposes. Claude (Anthropic, 2025), accessible at claude.ai, was used to assist with the correction of grammatical mistakes in the written text, as well as to enhance the visual quality of figures included in the thesis. All the presented intellectual content, analysis, interpretation, and conclusions are those of the author only.

References

Anthropic. (2025). *Claude Sonnet 4.6* (Accessed May 2026) [Large language model — used for grammar correction and image modification]. https://claude.ai

Andersson, O., & Gehlin, S. (2018). *State of the art: Sweden. Quality management in design and operation of borehole systems*. https://media.geoenergicentrum.se/2018/06/Andersson_Gehlin_2018_State-of-the-Art-report-Sweden-for-IEA-ECES-Annex-27.pdf

Ashry, I., Mao, Y., Wang, B., Hveding, F., Bukhamsin, A. Y., Ng, T. K., & Ooi, B. S. (2022). A Review of Distributed Fiber–Optic Sensing in the Oil and Gas Industry. *Journal of Lightwave Technology*, *40*(5), 1407–1431. https://doi.org/10.1109/JLT.2021.3135653

Bado, M. F., & Casas, J. R. (2021). A Review of Recent Distributed Optical Fiber Sensors Applications for Civil Engineering Structural Health Monitoring. *Sensors (Basel, Switzerland)*, *21*(5), 1818. https://doi.org/10.3390/s21051818

Betzig, E., Patterson, G. H., Sougrat, R., Lindwasser, O. W., Olenych, S., Bonifacino, J. S., Davidson, M. W., Lippincott-Schwartz, J., & Hess, H. F. (2006). Imaging Intracellular Fluorescent Proteins at Nanometer Resolution. *Science*, *313*(5793), 1642–1645. https://doi.org/10.1126/science.1127344

Bian, L., Wang, Z., Zhang, Y., Li, L., Zhang, Y., Yang, C., Fang, W., Zhao, J., Zhu, C., Meng, Q., Peng, X., & Zhang, J. (2024). A broadband hyperspectral image sensor with high spatio-temporal resolution. *Nature*, *635*(8037), 73–81. https://doi.org/10.1038/s41586-024-08109-1

Bohnert, K., Brandle, H., Brunzel, M., Gabus, P., & Guggenbach, P. (2005). Highly Accurate Fiber-Optic DC Current Sensor for the Electro-Winning Industry. *Record of Conference Papers Industry Applications Society 52nd Annual Petroleum and Chemical Industry Conference*, 121–128. Record of Conference Papers Industry Applications Society 52nd Annual Petroleum and Chemical Industry Conference. https://doi.org/10.1109/PCICON.2005.1524547

Bohnert, K., Gabus, P., Nehring, Jü., Brandle, H., & Brunzel, M. G. (2007). Fiber-Optic Current Sensor for Electrowinning of Metals. *Journal of Lightwave Technology*, *25*(11), 3602–3609. https://doi.org/10.1109/JLT.2007.906795

Boyd, R. W. (2019). *Nonlinear optics* (4th edn). Academic Press is an imprint of Elsevier.

Cook, H., Bezsudnova, Y., Koponen, L. M., Jensen, O., Barontini, G., & Kowalczyk, A. U. (2024). An optically pumped magnetic gradiometer for the detection of human biomagnetism. *Quantum Science and Technology*, *9*(3), 035016. https://doi.org/10.1088/2058-9565/ad3d81

da Costa, T. P., da Costa, D. M. B., & Murphy, F. (2024). A systematic review of real-time data monitoring and its potential application to support dynamic life cycle inventories. *Environmental Impact Assessment Review*, *105*, 107416. https://doi.org/10.1016/j.eiar.2024.107416

Dandu, P., Gusarov, A., Leysen, W., Beaumont, P., Wuilpart, M., & JET Contributors. (2023). Distributed Poloidal Magnetic Field Measurement in Tokamaks Using Polarization-Sensitive Reflectometric Fiber Optic Sensor. *Sensors*, *23*(13), 5923. https://doi.org/10.3390/s23135923

Dang, S., Zhang, B., Yang, Y., Song, Q., Zhang, D., Kong, Z., & Allahbakhsh, M. (2026). A Quantum-Based High-Precision Current Transducer for Smart Grid Applications. In H. Ma, J. She, B. Xin, & Q. Wang (Eds), *Advanced Computational Intelligence and Intelligent Informatics* (pp. 197–210). Springer Nature. https://doi.org/10.1007/978-981-95-6733-1_16

David A. Cremers, L. J. R. (2013). Handbook of Laser-Induced Breakdown Spectroscopy. In *Handbook of Laser-Induced Breakdown Spectroscopy* (pp. 29–68). John Wiley & Sons, Ltd. https://doi.org/10.1002/9781118567371.ch2

Diaspro, A., Chirico, G., & Collini, M. (2005). Two-photon fluorescence excitation and related techniques in biological microscopy. *Quarterly Reviews of Biophysics*, *38*(2), 97–166. https://doi.org/10.1017/S0033583505004129

Ding, Z., Guo, H., Liu, K., Hua, P., Zhang, T., Li, S., Liu, J., Jiang, J., & Liu, T. (2023). Advances in Distributed Optical Fiber Sensors Based on Optical Frequency-Domain

Reflectometry: A Review. *IEEE Sensors Journal*, *23*(22), 26925–26941. https://doi.org/10.1109/JSEN.2023.3317231

Ding, Z., Wang, C., Liu, K., Jiang, J., Yang, D., Pan, G., Pu, Z., & Liu, T. (2018). Distributed Optical Fiber Sensors Based on Optical Frequency Domain Reflectometry: A review. *Sensors*, *18*(4), 1072. https://doi.org/10.3390/s18041072

Evans, C. L., & Xie, X. S. (2008). Coherent Anti-Stokes Raman Scattering Microscopy: Chemical Imaging for Biology and Medicine. *Annual Review of Analytical Chemistry*, *1*(Volume 1, 2008), 883–909. https://doi.org/10.1146/annurev.anchem.1.031207.112754

Fedenko, V. S., Shemet, S. A., & Landi, M. (2017). UV–vis spectroscopy and colorimetric models for detecting anthocyanin-metal complexes in plants: An overview of in vitro and in vivo techniques. *Journal of Plant Physiology*, *212*, 13–28. https://doi.org/10.1016/j.jplph.2017.02.001

Giovannetti, V., Lloyd, S., & Maccone, L. (2004). Quantum-Enhanced Measurements: Beating the Standard Quantum Limit. *Science*, *306*(5700), 1330–1336. https://doi.org/10.1126/science.1104149

Gorji, R., Skvaril, J., & Odlare, M. (2024). Applications of optical sensing and imaging spectroscopy in indoor farming: A systematic review. *Spectrochimica Acta Part A: Molecular and Biomolecular Spectroscopy*, *322*, 124820. https://doi.org/10.1016/j.saa.2024.124820

Griffiths, P. R., & de HASETH, J. A. (n.d.). *Fourier Transform Infrared Spectrometry*.

Gusarov, A., Beaumont, P., & JET Contributors. (2025). Assessment of Neutron Radiation Effects on the Fiber Optics Current Sensor Performance During JET DTE2 Experimental Campaign. *Sensors*, *25*(21), 6552. https://doi.org/10.3390/s25216552

Gustafsson, M. G. L. (2000). Surpassing the lateral resolution limit by a factor of two using structured illumination microscopy. *Journal of Microscopy*, *198*(2), 82–87. https://doi.org/10.1046/j.1365-2818.2000.00710.x

Gutscher, M.-A., Cappelli, G., Quetel, L., Philippon, M., Lebrun, J.-F., Nativelle, C., Vitalis-Simon, S., & Autret, E. (2025). Monitoring Long-Term Seafloor Water

Temperature Changes Using Fiber Optic Sensing on Submarine Telecommunication Cables. *Geophysical Research Letters*, *52*(21), e2025GL119348. https://doi.org/10.1029/2025GL119348

Hell, S. W., & Wichmann, J. (1994). Breaking the diffraction resolution limit by stimulated emission: Stimulated-emission-depletion fluorescence microscopy. *Optics Letters*, *19*(11), 780–782. https://doi.org/10.1364/OL.19.000780

Hiltunen, E., Martinkauppi, B., Zhu, L., Mäkiranta, A., Lieskoski, M., & Rinta-Luoma, J. (2017). Renewable, carbon-free heat production from urban and rural water areas. *Journal of Cleaner Production*, *153*, 397–404. https://doi.org/10.1016/j.jclepro.2015.10.039

Karki, D., Khanikar, T., Mullurkara, S. V., Naeem, K., Hong, J. Y., & Ohodnicki, P. (2024). AC Magnetometry Using Nano-ferrofluid Cladded Multimode Interferometric Fiber Optic Sensors for Power Grid Monitoring Applications. *ACS Applied Nano Materials*, *7*(23), 26894–26906. https://doi.org/10.1021/acsanm.4c04912

Katrenova, Z., Alisherov, S., Abdol, T., & Molardi, C. (2024). Status and future development of distributed optical fiber sensors for biomedical applications. *Sensing and Bio-Sensing Research*, *43*, 100616. https://doi.org/10.1016/j.sbsr.2023.100616

Kazanskiy, N. L., Khonina, S. N., & Butt, M. A. (2023). Recent Development in Metasurfaces: A Focus on Sensing Applications. *Nanomaterials*, *13*(1), 118. https://doi.org/10.3390/nano13010118

Khonina, S. N., Kazanskiy, N. L., & Butt, M. A. (2023). Optical Fibre-Based Sensors—An Assessment of Current Innovations. *Biosensors*, *13*(9). https://doi.org/10.3390/bios13090835

Klar, T. A., Jakobs, S., Dyba, M., Egner, A., & Hell, S. W. (2000). Fluorescence microscopy with diffraction resolution barrier broken by stimulated emission. *Proceedings of the National Academy of Sciences*, *97*(15), 8206–8210. https://doi.org/10.1073/pnas.97.15.8206

Knight, J. W., Egan, J. V., Orr-Ewing, A. J., & Cotterell, M. I. (2022). Direct Spectroscopic Quantification of the Absorption and Scattering Properties for Single Aerosol

Particles. *The Journal of Physical Chemistry A*, *126*(9), 1571–1577. https://doi.org/10.1021/acs.jpca.2c00532

Li, J., & Zhang, M. (2022). Physics and applications of Raman distributed optical fiber sensing. *Light: Science & Applications*, *11*(1), 128. https://doi.org/10.1038/s41377-022-00811-x

Liang, H., Wang, J., Zhang, L., Liu, J., & Wang, S. (2022). Review of Optical Fiber Sensors for Temperature, Salinity, and Pressure Sensing and Measurement in Seawater. *Sensors (Basel, Switzerland)*, *22*(14), 5363. https://doi.org/10.3390/s22145363

Liu, H., Guo, H., Tan, M., Li, Q., Meng, X., & Yang, X. (2022). Accurate optical fiber current transducer for high-voltage direct current (HVDC) transmission. *Instrumentation Science & Technology*, *50*(6), 604–615. https://doi.org/10.1080/10739149.2022.2053152

Loskutova, A., Seitkali, A., Aliyev, D., & Bukasov, R. (2025). Quantum Dot-Based Luminescent Sensors: Review from Analytical Perspective. *International Journal of Molecular Sciences*, *26*(14), 6674. https://doi.org/10.3390/ijms26146674

Mahmud, R. A., Arebu, H. A., Khan, M. Z. M., & Qureshi, K. K. (2024). Recent Applications of Tapered Multicore Fiber in Optical Sensing: A Review. *IEEE Sensors Journal*, *24*(15), 23376–23388. https://doi.org/10.1109/JSEN.2024.3416037

Mäkiranta, A. (2020). Renewable thermal energy sources: Sediment and asphalt energy applications in an urban northern environment. Vaasan yliopisto. https://osuva.uwasa.fi/handle/11111/4092

Mandl, J., Trampitsch, P., Fröhlich, A., Klambauer, R., & Bergmann, A. (2026). Detection of geomagnetically induced currents on single phases in power grids using a fiber optic current sensor system. *Journal of Sensors and Sensor Systems*, *15*(1), 1–8. https://doi.org/10.5194/jsss-15-1-2026

Meng, Y., Yang, Z., & Wang, L. (2026a). A Review of Optical Sensor Applications in Water, Atmospheric and Soil Environmental Monitoring. In A. Grangetto, A. G. Martínez, E. A. Castro Rojas, & A. J. Tallón-Ballesteros (Eds), *Frontiers in Artificial Intelligence and Applications*. IOS Press. https://doi.org/10.3233/FAIA260023

Meng, Y., Yang, Z., & Wang, L. (2026b). A Review of Optical Sensor Applications in Water, Atmospheric and Soil Environmental Monitoring. In *Machine Learning and Artificial Intelligence* (pp. 158–163). IOS Press. https://doi.org/10.3233/FAIA260023

Mia, N., Hashem, Md. A., Halim, Md. A., Tariq, S., & Ahamed, Z. (2026). Application of NIR spectroscopy with machine learning in the food industry: A comprehensive review. *Food Physics*, 100089. https://doi.org/10.1016/j.foodp.2026.100089

Palmieri, L., Sarchi, D., & Galtarossa, A. (2015). Distributed measurement of high electric current by means of polarimetric optical fiber sensor. *Optics Express*, *23*(9), 11073–11079. https://doi.org/10.1364/OE.23.011073

Pathak, A. K., & Viphavakit, C. (2022). A review on all-optical fiber-based VOC sensors: Heading towards the development of promising technology. *Sensors and Actuators A: Physical*, *338*, 113455. https://doi.org/10.1016/j.sna.2022.113455

Pelaez Quiñones, J. D., Sladen, A., Ponte, A., Lior, I., Ampuero, J.-P., Rivet, D., Meulé, S., Bouchette, F., Pairaud, I., & Coyle, P. (2023). High resolution seafloor thermometry for internal wave and upwelling monitoring using Distributed Acoustic Sensing. *Scientific Reports*, *13*(1), 17459. https://doi.org/10.1038/s41598-023-44635-0

Pellegrini, S., Rizzelli, G., Andrenacci, L., Minelli, L., Pilori, D., Bosco, G., Crognale, C., Piciaccia, S., Tanzi, A., & Gaudino, R. (2024). Polarization-based Optical Fiber Sensing: A State of the Art Review. *2024 Italian Conference on Optics and Photonics (ICOP)*, 1–4. https://doi.org/10.1109/ICOP62013.2024.10803652

Petrenko, M., & Vershovskii, A. (2022). Towards a Practical Implementation of a Single-Beam All-Optical Non-Zero-Field Magnetic Sensor for Magnetoencephalographic Complexes. *Sensors*, *22*(24), 9862. https://doi.org/10.3390/s22249862

Rashed, A. K., Alshehawy, A. M., Mansour, D.-E. A., Farade, R. A., Ghali, M., & Megahed, T. F. (2025). Optical Spectroscopy Techniques for Condition Assessment and Fault Diagnosis of Power Transformer Insulation: A Critical Review on Technologies, Methods, and Standards. *IEEE Transactions on Dielectrics and Electrical Insulation*, *32*(4), 2162–2176. https://doi.org/10.1109/TDEI.2025.3538816

Rondin, L., Tetienne, J.-P., Hingant, T., Roch, J.-F., Maletinsky, P., & Jacques, V. (2014). Magnetometry with nitrogen-vacancy defects in diamond. *Reports on Progress in Physics*, *77*(5), 056503. https://doi.org/10.1088/0034-4885/77/5/056503

Rui, Y., Hird, R., Yin, M., & Soga, K. (2019). Detecting changes in sediment overburden using distributed temperature sensing: An experimental and numerical study. *Marine Geophysical Research*, *40*(3), 261–277. https://doi.org/10.1007/s11001-018-9365-4

Rust, M. J., Bates, M., & Zhuang, X. (2006). Sub-diffraction-limit imaging by stochastic optical reconstruction microscopy (STORM). *Nature Methods*, *3*(10), 793–796. https://doi.org/10.1038/nmeth929

Sabri, N., Aljunid, S. A., Salim, M. S., Ahmad, R. B., & Kamaruddin, R. (2013). Toward Optical Sensors: Review and Applications. *Journal of Physics: Conference Series*, *423*(1), 012064. https://doi.org/10.1088/1742-6596/423/1/012064

Senkans, U., Silkans, N., Merijs-Meri, R., Haritonovs, V., Skels, P., Porins, J., Lima, M. S. S., Spolitis, S., Braunfelds, J., & Bobrovs, V. (2026). Fiber-Optical-Sensor-Based Technologies for Future Smart-Road-Based Transportation Infrastructure Applications. *Photonics*, *13*(2). https://doi.org/10.3390/photonics13020106

Sing Muk, N. (2019). Carbon Dots as Optical Nanoprobes for Biosensors. In *Nanobiosensors for Biomolecular Targeting* (pp. 269–300). Elsevier. https://doi.org/10.1016/B978-0-12-813900-4.00012-9

Su, Y.-D., Preger, Y., Burroughs, H., Sun, C., & Ohodnicki, P. R. (2021). Fiber Optic Sensing Technologies for Battery Management Systems and Energy Storage Applications. *Sensors*, *21*(4), 1397. https://doi.org/10.3390/s21041397

Taha, B. A. (2021). Comprehensive Review Tapered Optical Fiber Configurations for Sensing Application: Trend and Challenges. *Biosensors (Basel)*, *11*(8), 253-. https://doi.org/10.3390/bios11080253

Udd, E., & Jr, W. B. S. (2024). Fiber Optic Sensors: An Introduction for Engineers and Scientists. John Wiley & Sons.

Van de Giesen, N., Steele-Dunne, S. C., Jansen, J., Hoes, O., Hausner, M. B., Tyler, S., & Selker, J. (2012). Double-Ended Calibration of Fiber-Optic Raman Spectra

Distributed Temperature Sensing Data. *Sensors*, *12*(5), 5471–5485. https://doi.org/10.3390/s120505471

Wadi Harun, S. (Ed.). (2025). *Optical Technologies for Advancing Communication, Sensing, and Computing Systems*. IntechOpen. https://doi.org/10.5772/intechopen.1003549

Wagner, G. A., & Plusquellic, D. F. (2016). Ground-based, integrated path differential absorption LIDAR measurement of CO_2, CH_4, and H_2O near 1.6 µm. *Applied Optics, Vol. 55, Issue 23, Pp. 6292-6310*. https://doi.org/10.1364/AO.55.006292

Wang, R., Li, H., Liu, C., Dai, J., Cheng, C., Hu, W., & Yang, M. (2026). Review of Fiber Optic Sensing Technologies for Leak Detection in Hydrogen Energy Storage and Transport Equipment. *IEEE Sensors Reviews*, *3*, 219–242. https://doi.org/10.1109/SR.2026.3652038

Wu, J., Zhang, X., Chen, L., Wu, B., & Peng, C. (2022). Research on All-Fiber Dual-Modulation Optic Current Sensor Based on Real-Time Temperature Compensation. *IEEE Photonics Journal*, *14*(3), 1–9. https://doi.org/10.1109/JPHOT.2022.3162114

Xiao, C., Long, J., Jiang, L., Yan, G., & Rao, Y. (2022). Review of Sensitivity-enhanced Optical Fiber and Cable Used in Distributed Acoustic Fiber Sensing. *2022 Asia Communications and Photonics Conference (ACP)*, 359–363. https://doi.org/10.1109/ACP55869.2022.10089130

Zhang, J.-W., Meng, X., Han, T., Wei, X., Wang, L., Zhao, Y., Fu, G., Tian, N., Wang, Q., Qin, S., Liu, X., & Putson, C. (2023). Optical magnetic field sensors based on nanodielectrics: From biomedicine to IoT-based energy internet. *IET Nanodielectrics*, *6*(3), 116–129. https://doi.org/10.1049/nde2.12049

Zhao, Y., Yin, B., Sang, G., Jiang, Z., Li, H., Wu, B., Pei, L., & Wu, S. (2025). Applications of optical fiber sensors in marine observation: A review. *Intelligent Marine Technology and Systems*, *3*(1), 38. https://doi.org/10.1007/s44295-025-00089-w

Zhu, P., Hu, Z., Li, H., Dai, M., Chen, J., Hu, Z., & Xu, X. (2026). Underwater Noise in Offshore Wind Farms: Monitoring Technologies, Acoustic Characteristics, and

Long-Term Adaptive Management. *Journal of Marine Science and Engineering*, *14*(3). https://doi.org/10.3390/jmse14030274

Zhuang, F., Li, Y., Guo, T., Yang, Q., Luo, Y., Wang, J., & Wang, S. (2024). Review on In-Situ Marine Monitoring Using Physical and Chemical Optical Fiber Sensors. *Photonic Sensors*, *15*(2), 250230. https://doi.org/10.1007/s13320-024-0731-3